TITLE: Grouping behavior in a Triassic marine apex predator

AUTHORS: Neil P. Kelley[1,2,*], Randall B. Irmis[3], Paige E. dePolo[4,5], Paula J. Noble[5], Danielle Montague-Judd[3,6], Holly Little[2], Jon Blundell[7], Cornelia Rasmussen[3,8], Lawrence Percival[9,10], Tamsin A. Mather[10], Nicholas D. Pyenson[2]

AFFILLIATIONS:

[1-] Current mailing address: Department of Earth and Environmental Sciences, Vanderbilt University, PMB 351805 2301 Vanderbilt Place, Nashville, TN 37235-1805 USA

[2-] Department of Paleobiology, National Museum of Natural History, Smithsonian Institution, 1001 Madison Drive NW, Washington DC, 20560 USA

[3-] Department of Geology and Geophysics and Natural History Museum of Utah, University of Utah, 115 S 1460 E, Salt Lake City, UT 84112 USA

[4-] School of GeoSciences, University of Edinburgh, Drummond St, Edinburgh EH8 9XP United Kingdom

[5-] Department of Geological Sciences and Engineering, University of Nevada—Reno, 1664 N. Virginia Street, Reno, NV 89557 USA

[6-] Department of Geosciences, University of Arizona, 1040 E 4th St, Tucson, AZ 85721 USA

[7-] Digitization Program Office 3D Lab, Office of the Chief Information Officer, Smithsonian Institution, Landover, MD 20758 USA

[8-] Institute for Geophysics, Jackson School of Geosciences, University of Texas at Austin, 2305 Speedway Stop C1160, Austin, TX 78712-1692 USA

[9-] Analytical, Environmental and Geochemistry Group (AMGC), Vrije Universiteit Brussel, Pleinlaan 2 Brussels 1050, Belgium

[10-] Department of Earth Sciences, University of Oxford, South Parks Road, Oxford OX1 3AN, UK

*Corresponding author and lead contact: neil.p.kelley@vanderbilt.edu

SUMMARY

Marine tetrapods occupy important roles in modern marine ecosystems and often gather in large aggregations driven by patchy prey distribution[1,2], social or reproductive behaviors[3,4] or oceanographic factors[5]. Here, we show that similar grouping behaviors evolved in an early marine tetrapod lineage, documented by dozens of specimens of the giant ichthyosaur *Shonisaurus* in the Luning Formation in West Union Canyon, Nevada, USA[6,7]. A concentration of at least seven skeletons closely preserved on a single bedding plane received the bulk of previous attention. However, many more specimens are preserved across ~10^6 square meters and ~200 stratigraphic meters of outcrop representing an estimated >$10^{5–6}$ years. Unlike other marine tetrapod rich deposits, this assemblage is essentially monotaxic; other vertebrate fossils are exceptionally scarce. Large individuals are disproportionately abundant, with the exception of multiple neonatal or embryonic specimens, indicating an unusual demographic composition apparently lacking intermediate-sized juveniles or subadults. Combined with geological evidence, our data suggest dense aggregations of *Shonisaurus* inhabited this moderately deep, low-diversity, tropical marine environment for millennia during the latest Carnian Stage of the Late Triassic (237-227 Ma). Thus, philopatric grouping behavior in marine tetrapods, potentially linked to reproductive activity, has an antiquity of at least 230 million years.

Results and Discussion

Marine tetrapods are ecologically important members of ocean ecosystems, directly influencing nutrient cycling and ecosystem structure, in part because of their relatively large body sizes and high mobility [8,9]. Top marine predators today frequently coordinate seasonal migrations, forming

transient aggregations or persistent social groups, with effects that further modulate their impacts on marine ecosystems. Understanding the significance of these ecological dynamics over geologic time scales requires fossil data[10,11]. Fossil sites with exceptional abundance and/or preservation can provide critical ecological snapshots that are otherwise unavailable. However, investigations into the genesis of exceptional marine tetrapod-bearing deposits have often focused on the physical and environmental controls on fossil accumulation and preservation[12,13]. In contrast, the insights into behavioral and ecological dynamics provided by marine tetrapod fossil assemblages have received much less attention.

The Luning Formation at Berlin-Ichthyosaur State Park (BISP) in West Union Canyon (WUC), central Nevada, U.S.A., contains an unusual marine tetrapod assemblage preserving dozens of associated skeletons and fragmentary specimens of the Late Triassic giant ichthyosaur *Shonisaurus popularis*[6,7]. Though individuals of *Shonisaurus* have been discovered at multiple sites across ~2 km^2 in WUC (Figure 1, Figure S2), most attention since the mid 20^{th} century has focused on a high concentration of articulated skeletons left *in situ* on a single bedding plane, called Quarry 2 (Figures 1 and 2, Figure S1). Hypotheses ranging from stranding to mass mortality have been proposed for the skeletal concentration at Quarry 2, but none of them are well-supported by geologic or taphonomic evidence.[6,7,14] Beyond Quarry 2, the broader significance of the abundance of *Shonisaurus* and the dearth of other marine vertebrate taxa across multiple horizons within the Luning Formation at WUC remains poorly understood.

Geology, Geochemistry and Taphonomy

We investigated the geology and taphonomy of previously known localities including Quarry 2 and the *Shonisaurus* type locality (Quarry 5) and surveyed the distribution of vertebrate fossils across WUC (Figure 1b). We identified and georeferenced 112 vertebrate specimens from

50 distinct localities including the *in situ* specimens in Quarry 2 (Table 1, GPS coordinates of all localities on file with UMNH). *Shonisaurus* occurs at multiple horizons within two members of the Luning Formation, spanning three ammonoid zones[15]. Though specimens referable to *Shonisaurus* are present in three ammonoid zones (Figure 1c), the majority are from the latest Carnian *Klamathites macrolobatus* zone, including Quarry 5 and the bonebed at Quarry 2, clarifying a discrepancy among previous descriptions[6,7,14]. Except for a few non-diagnostic bone fragments, we identify all tetrapod occurrences as ichthyosaurian based on porous bone texture lacking an outer cortical layer[16]. Moreover, all diagnostic elements invariably showed additional features typical of *Shonisaurus*, including massive ribs with a round cross-section, very large amphicoelous vertebral centra with a high width-to-length ratio and lacking attached neural arches, massive and distinctive limb and girdle elements, including sub-rectangular humeri and proximally expanded coracoids, and deep jaw fragments bearing large teeth with highly infolded roots set in distinct sockets (Figure 3a–e)[6,17]. Non-ichthyosaur macrovertebrate specimens are exceedingly scarce, comprising two elasmobranch fin spines, small osteichthyan bones and indeterminate bone fragments (Table 1), consistent with what has been previously reported for the site[6].

Fossil-bearing strata at BISP comprise organic mudstones interspersed with thinner carbonate horizons; the latter units are predominantly wackestones and packstones with abundant disarticulated bivalves, echinoids and other invertebrates. This sedimentology is consistent across ichthyosaur-bearing horizons and suggests deposition below fair-weather wave base, but above maximum storm wave base (Figure S4, Methods S1). *Shonisaurus* fossils are present in both mudstone and carbonate facies (Figure 1c). This moderately deep distal ramp setting[cf. 7] excludes an earlier hypothesis of stranding for the ichthyosaur assemblage[6], unless stranded

carcasses were transported to deeper water *en masse*, an unlikely hypothesis that is difficult to test. There is no direct geological evidence for a major environmental perturbation (e.g., ocean anoxia, carbon cycle changes or volcanic eruptions) either coeval with or immediately prior/following deposition of the Quarry 2 bonebed that might provide a repeated kill mechanism. The latest Carnian *macrolobatus* zone post-dates the Carnian Pluvial Episode (CPE) by at least 2-3 million years[18], but is within known uncertainties for the eruption of the Wrangellia flood basalts (~234–225 Ma)[19]. Although there is some variability above and below the bonebed in Quarry 2, the *Shonisaurus*-rich layer itself shows no evidence of a clear mercury (Hg) peak or increased enrichment with respect to total organic carbon (i.e., increased Hg/TOC) that would imply a large subaerial eruptive event as a driver of increased ichthyosaur mortality and would result in the preserved fossil assemblage at that site (Figure S3, Methods S1). This absence of a clear peak contrasts with the more coherent signals attributed to the Wrangellia eruptions observed in more distal western Tethys successions associated with the CPE itself[20]. Similarly, *Shonisaurus*-bearing horizons in Quarries 2 and 5 do not stratigraphically correlate with any observed excursions in the organic carbon isotope ($\delta^{13}C_{org}$) record. Though negative $\delta^{13}C_{org}$ excursions can record disruption of primary productivity or a flux of isotopically light carbon to the ocean-atmosphere system[21], the most negative values in WUC are not associated with ichthyosaur-rich horizons, and nor are large-scale carbon cycle perturbations thought to have occurred during the late Carnian. Instead, the high total organic carbon (TOC) contents of samples with lower $\delta^{13}C_{org}$ values suggests that they likely reflect locally increased carbon burial (Figure 1d–e; Figure S3, Methods S1), or a change in the aggregate composition of organic matter. Thus, we find no clear evidence for a persistent environmental mechanism biased towards killing or preserving *Shonisaurus*.

Although most occurrences of *Shonisaurus* within WUC are isolated individuals, in at least three localities (Figure S2, Table S3) multiple individuals occur in proximity sometimes on the same stratigraphic level. This is most striking at Quarry 2 where we identified twelve distinct clusters of associated or articulated bones (Figure 2a, Figure S1, Tables 1 and S3). Some of these likely represent multiple portions of the same animal fragmented by taphonomic processes. Four partial skulls with associated pectoral girdles provide a conservative minimum number of individuals. Based on position and arrangement of clusters we estimate that at least seven individuals are preserved in the quarry (Figure 2d), although previous estimates of nine individuals[7] cannot be conclusively rejected. Original excavations revealed as many as six additional partial skeletons near Quarry 2[6] (Figure S2); these could represent an extension of the bone bed, but the fate of most of this material is unknown and the limited available information renders this hypothesis equivocal. Though the Quarry 2 specimens are all associated, their taphonomic condition ranges widely (Figure 2b). Most clusters within Quarry 2 exhibit a parallel alignment (Figure 2c) and are lacking smaller elements including distal limbs and tail, suggesting variably moderate-to-high degrees of decay, disarticulation and hydraulic modification prior to burial. Petrographic analysis of the bone-bearing carbonate layer in Quarry 2 shows a dense concentration of broken invertebrate shell fragments with preferential alignment subparallel to bedding in a fine-grained carbonate mud matrix (Figure S4, Methods S1), consistent with transient elevated energy levels below fair-weather wave base, and similar to the sedimentology observed at quarries 5 and 6. Differential degrees of articulation and completeness reflect varying degrees of decay prior to burial and suggest that some carcasses were either floating in the water column or sitting on the seabed for some time prior to burial[22].

In contrast, at other WUC *Shonisaurus* sites, specimens show a wider range of taphonomic conditions. Apart from Quarry 2, at least four other localities are known to preserve partially articulated skeletons including the original type locality and a newly discovered site (Figure S2, Table S3). However, isolated bones found *in situ* at multiple locations in WUC demonstrate that some skeletons were fully disarticulated prior to burial. Articulated remains appear to be more common in the *macrolobatus* zone, which coincides with an overall maximum abundance of *Shonisaurus* occurrences, including isolated and disarticulated remains (Figure 1c). Original excavations documented fragmentary but associated or partially articulated remains in the underlying *schucherti* zone[6]; however, *Shonisaurus* fossils are more sparsely distributed in these lower horizons, and we did not discover additional articulated remains within this interval (Figure 1c, Table 1).

Age Structure

The majority of *Shonisaurus* specimens from WUC represent very large individuals spanning a narrow size class, both in Quarry 2 and at other WUC localities, based on comparisons of humerus length (a frequently used proxy for body size in ichthyosaurs[23–25]) and other skeletal proportions (Figure 3f, g, Table S1). Humeri within Quarry 2 range from 31 to 45 cm in length and all others known from WUC fall within this range. Based on previously published correlations between ichthyosaur humerus length and total body length, this corresponds to total estimated body lengths of WUC *Shonisaurus* ranging from 11–16 m, consistent with earlier estimates[6,17,26]. The restricted size distribution across WUC *Shonisaurus* specimens, limited to very large individuals, contrasts with other marine reptile lagerstätten which preserve a more complete postnatal ontogenetic sample including juveniles, subadults, and adults[28–30].

Although the vast majority of *Shonisaurus* occurrences in WUC represent large, skeletally mature individuals, we identified three discrete occurrences representing embryonic or neonatal individuals. One specimen (NSMLV VM-2014-057-FS-001) consists of a mass of small bones from the pelvic region of the type *Shonisaurus* specimen (Figure 3h, Supplemental Information); it was previously noted in the original description of the taxon[6] but never figured or described in detail. Another small isolated centrum associated with the type material was identified in collections (NSMLV VM-2014-057-FS-007, Figure S5b). Our µCT analyses confirm the identification of these elements as extremely small *Shonisaurus* vertebrae, based on their high diameter to length ratio and overall similarity in shape and proportion to adult *Shonisaurus* centra (Supplemental Information). A very small surface-collected, isolated vertebral centrum (UMNH VP 32547, Figure S5c) found in a different area of WUC is a close match with those found *in situ* within the type specimen (Supplemental Information). Finally, a surface-collected fragmentary jaw (UCMP 290269) exhibits teeth with heavily plicated roots set in discrete sockets separated by thin bony partitions consistent with the distinctive dentition observed in adult *Shonisaurus popularis* (Figure 3a–e, Figure S5a). Thus, the size distribution of the WUC *Shonisaurus* assemblage is markedly bimodal, with large individuals and embryos/neonates, but no observed intermediately sized juveniles (Figure 3f,g).

Paleoecological Implications

The large size of *Shonisaurus*, together with new specimens preserving robust sectorial teeth throughout the jaws (Figure 3d, e), indicate a trophic role as a macrophagous raptorial predator that likely fed at least in part on large-bodied prey, i.e. the so called 'cut guild'[30], as opposed to previous suggestions of specialized filter feeding[31] or suction feeding[32]. However, there are very few potential large prey items preserved within the Luning Formation at WUC.

This scarcity does not appear to be due to preservation bias as large *Shonisaurus* and small invertebrate fossils, including ammonoids and bivalves, are very abundant at the site. We therefore propose that *Shonisaurus* likely fed elsewhere, consistent with wide ranging foraging activities of most large extant marine tetrapods[8]. Indeed, *Shonisaurus* fossils are also abundant in other Luning Fm. exposures about 60 km southwest of WUC in the Pilot Mountains of Nevada[33,34], suggesting a broader regional distribution within the partially restricted seaway in which these marine sediments were deposited. Outside of the Luning Fm., specimens referred to *Shonisaurus* occur in other Late Triassic marine deposits associated with accreted arc terranes preserved in Sonora, Mexico[35,36], southeastern Alaska[37], and possibly northern California[36]. Despite lower sample sizes, outside of the Luning Fm. *Shonisaurus* occurs in association with other marine reptile taxa and other vertebrates, and likely occupied a top-predator role in multi-tiered marine food webs (Figure 1a). The large size of *Shonisaurus* is also consistent with long distance travel, as the co-evolution of migration and body size, modulated by dynamics such as climate and patchy prey distribution, has been suggested for other marine tetrapod clades[38].

Abundant *Shonisaurus* fossil occurrences in WUC span approximately 200 m of section and more than a complete ammonoid biozone representing $>10^{5–6}$ years[39] (Figure 1c, Supplemental Information). The preponderance of large individuals, the scarcity of other large marine vertebrate fossils, the presence of both *in situ* and isolated embryonic or neonatal specimens, and records of *Shonisaurus* from other approximately coeval localities spanning ~30 degrees of paleolatitude and a range of paleoenvironments (Figure 1a) are all consistent lines of evidence with a scenario tied to reproductive aggregation and/or seasonal migration. This scenario involves sexually mature, in some cases gravid, individuals aggregating together in groups in the absence of potential predators that would target newborns. These dense

aggregations would have been vulnerable to mortality events and subsequent burial penecontemporaneously, as observed at Quarry 2, although many WUC *Shonisaurus* occurrences, which range from isolated and disarticulated to nearly complete specimens at multiple stratigraphic levels, likely represent attritional mortality. Thus, although Quarry 2 is notable in preserving a large number of associated skeletons, it is representative of the larger-scale pattern of an essentially monotypic marine tetrapod assemblage of *Shonisaurus* throughout WUC.

Although the WUC assemblage is far from unique in preserving ichthyosaur embryos[40–42] it does contrast with most other ichthyosaur-bearing lagerstätten by the absence other marine reptile taxa, even other species of ichthyosaurs, and scarcity of intermediate-sized juveniles or subadults. However, it is possible that grouping behavior linked to seasonal reproductive cycles played a role in the genesis of other ichthyosaur-rich fossil assemblages. Notably, group migratory behavior is a common feature of many extant marine tetrapods and other large marine vertebrates. For example, baleen whales seek out lower productivity water to give birth, either to avoid potential predators[43] or for energetic reasons[44].

Conclusion

The Mesozoic Era marks a pivotal interval in the modernization of marine and terrestrial ecosystems across all trophic levels[45,46]. This transition was initiated during the Triassic, in the wake of the end-Permian mass extinction. By the Middle Triassic, five million years later, ichthyosaurs evolved the large body sizes typical of dominant predators at the top of marine food webs[47,48]. This role has been occupied by successive lineages of marine tetrapod predators ever since, punctuated by turnovers driven by extinctions and radiations of new marine clades[49]. Triassic ichthyosaurs were among the first marine tetrapods to acquire key innovations, such as

high-performance swimming[50], deep diving[51,52] and aquatic birth[40], many of which evolved convergently among other Mesozoic marine reptiles and over 130 million years later in seabirds and marine mammals.

The results presented here underscore an additional behavioral trait that emerged early in ichthyosaur evolution: grouping behavior of adults. The ichthyosaur aggregations recorded in the Luning Formation at WUC seem to have occurred in the absence of an abundant prey source, suggesting *Shonisaurus* might have regularly travelled between birthing and feeding grounds. Similar mass movements are observed in the life history of many marine tetrapods today, including whales[53], pinnipeds[3], and penguins[4]. Grouping behaviors of large marine predators amplify their impacts on ecosystems and their long-distance movements link spatio-temporally distinct habitats. Our results suggest that marine tetrapods have participated in these dynamics for more than 230 million years.

Acknowledgements WUC is within the ancestral homelands of the Numu (Notherrn Paiute) and Newe (Western Shoshone) peoples. This research was conducted under research permits issued by and with assistance from the U.S. Forest Service (Humboldt-Toiyabe National Forest) and Nevada State Parks. Funding was provided by Smithsonian Institution, University of Nevada-Reno, Vanderbilt University, and University of Utah. We thank numerous volunteers and students from all institutions for assistance with fieldwork and fossil preparation as well as data processing; R. Johnson prepared the elements of UMNH VP 32539 in Figure 3. T. Birthisel and C. Levitt-Bussian (UMNH) provided assistance in the field, lab, and with curation. S. Underwood (NVSMLV), D. Smith, P. Holroyd (UCMP), and J. Morris (BISP) provided access to archives and collections under their care and facilitated loan of material. B. Gibson (Vanderbilt University) assisted with µCT scanning. Steve Wyatt (University of Oxford) and K Ritterbush (University of Utah) generously provided access to analytical equipment under their care. M. Dattoria, V. Rossi (Smithsonian) and K. Kunze (QuietPixel) assisted with 3D models. L. Delsett, A. Friedlaender and T. Faith provided feedback on an earlier version of the manuscript. Valentin Fischer and two anonymous reviewers provided helpful suggestions to improve the manuscript. We thank T. Young (Great Basin Brewing) for his continued support and unending enthusiasm and the late R. Riggs (BISP) for his service as an ambassador and caretaker of unique fossil resources.

Author Contributions N.K., N.P., R.B.I., P.N. and P.dP. designed the study, collected and analyzed data. H.L. and J.B. collected and processed photogrammetry and laser scan data. C.R., L.P. and T.M. collected and analyzed geochemical data. D.M-J. and C.R. provided assistance in

the field and D.M-J. provided access to previously unpublished data and identified invertebrate fossils. N.K. wrote the manuscript draft with help from N.P. and R.B.I. and all authors provided input and edits.

Declaration of Interests The authors report no competing interests.

Inclusion and Diversity We support inclusive, diverse, and equitable conduct of research

Main-text Figures and Table Legends

Figure 1. Geographic, geologic and stratigraphic context of ichthyosaur occurrences at WUC. (A) Paleogeography of the Late Triassic adapted from[54] indicating the distribution of *Shonisaurus* and other marine reptiles. Pie charts denote major assemblages, squares mark isolated occurrences; **(B)** geologic map of West Union Canyon (WUC) adapted from[14], dotted areas denote where *Shonisaurus* fossils have been found in WUC; **(C)** Summarized stratigraphy of WUC based on refs. [14] and [15], indicating the occurrence of *Shonisaurus* and other vertebrate fossils, stratigraphic position of Quarry 2 (Q2) and Quarry 5 (Q5) is approximate. ms = mudstone, ss = sandstone, ls = limestone, cg = conglomerate; **(D)** and **(E)** stratigraphy and geochemistry of key sites within WUC Quarry 2 (mass mortality) and Quarry 5 (type locality), blue bars indicate ichthyosaur bearing horizons. See also Table 1, Figures S2, S3 and S4, Table S2 and Methods S1.

Figure 2. Taphonomic interpretation of Quarry 2. (A) Orthographic view of mass mortality layer (Quarry 2) generated by photogrammetry and laser scanning; **(B)** taphonomic state of Quarry 2 skeletons by skeletal region, half-filled boxes <50% complete, filled boxes >50% complete, sk=skull, pec=pectoral girdle, fl=forelimb, tr=trunk, hl=hindlimb, ta=tail; **(C)** rose diagram indicating directional orientation of skeletal units; **(D)** interpretation of mass mortality layer; Roman numerals designate discrete skeletons; **(E)** sequence showing successive stages of disarticulation of vertebral columns, white rectangles on panel a indicate position of each view. See also Figures S1 and S2 and Table S3.

Figure 3. Select ichthyosaur fossils from WUC illustrating overall size distribution and anatomy. (A) Lower jaw (dentary) from adult *Shonisaurus* (UMNH VP 32539); **(B)** above: embryo or neonate jaw (UCMP 290269), below: µCT scan of same showing five alveoli and two *in situ* infolded tooth-roots; **(C)** µCT of adult *Shonisaurus* jaw (BISP 10); **(D)** Complete tooth from UMNH VP 32539 showing characteristic features including deep, infolded root and carinae; **(E)** Partial jaw (UMNH VP 32535) with *in situ* tooth missing distal tip of crown; **(F)** dimensions of largest vertebral centra, colored specimens indicate Quarry 2 specimens (vertebrae shown is from BISP Quarry 2 Specimen III) starred specimens embryo or neonatal material (NVSM-LV VM-2014-057-FS-001 shown); **(G)** comparison of humerus and coracoid lengths, colored specimens are Quarry 2 specimens following colors of Figure 2; **(H)** above: *in situ* embryo vertebrae within posterior rib block of *Shonisaurus* holotype (NVSM-LV VM-2014-057-FS-001), below: interpretive line drawing of *in situ* embryo remains, yellow bones were removed for µCT scanning (shown in panel f, and Supplemental Information), gray bones have not yet been prepared or scanned, brown stippled regions shows area partially covered by matrix. See also Figure S4, Table S1 and Methods S1.

Table 1. West Union Canyon vertebrate fossil specimens by ammonoid zone and taphonomic state. See also Table S3 and Methods S1.

STAR Methods

RESOURCE AVAILABILITY

Lead contact

Correspondence and requests for materials should be addressed to Neil Kelley, neil.p.kelley@vanderbilt.edu

Materials availability

This study did not generate new unique reagents

Data availability

Fossil locality data are not publicly available, but kept on file at UMNH along with geologic samples and thin sections. Fossils included in this manuscript are identified by specimen number and available for study with permission from their home institution (see below).
The µCT datasets generated by the current study are available at Morphosource: https://www.morphosource.org/projects/000476372 and 3D surface data at: https://3d.si.edu/object/3d/25748134-a3ec-4a4a-868b-8192ec73f6a6. The 3D model is also catalogued in the collections of the Smithsonian National Museum of Natural History: http://n2t.net/ark:/65665/33ca0e041-4ae9-4b74-bfab-fd9885f2dffa.

Code availability

This paper does not report original code.

Any additional information required to reanalyze the data reported in this paper is available from the lead contact upon request.

EXPERIMENTAL MODEL AND SUBJECT DETAILS

Museum abbreviations

BISP – Berlin-Ichthyosaur State Park; NVSMLV – Nevada State Museum, Las Vegas; UMNH – Utah Museum of Natural History; UCMP – University of California Museum of Paleontology

Information about the specimens

Fossils in Quarry 2 were digitized but otherwise left undisturbed *in-situ*. Newly collected fossil material is reposited at UMNH under permit agreement with the United States Forest Service. Additional data was acquired from previously collected material reposited at NVSMLV, UCMP and BISP as well as from additional published and unpublished sources see details below and in supplemental materials. All diagnostic reptile fossils we examined are referrable to *Shonisaurus*.

METHOD DETAILS

Capturing, processing and rendering 3D digital datasets

We documented *in situ* skeletal remains of *Shonisaurus* in Quarry 2 using three-dimensional digitization techniques. Photogrammetry datasets were captured using a prime 35mm Canon L series lens on a Canon 5D Mark III camera body. Scale was set for the photogrammetry data

using scale bars designed by the Bureau of Land Management and produced and calibrated by Cultural Heritage Imaging. We also used a FARO Focus 3D X 330 medium range spherical laser scanner to supplement the photogrammetry data sets and to verify the scale, topography, and alignment of the 3D model derived from the photogrammetry data sets. We used X-Rite ColorChecker targets for color calibration of the photogrammetry image sets and produced color corrected images using the X-Rite ColorChecker software and Adobe Camera Raw. Agisoft PhotoScan 1.2 was used for photogrammetry model creation; Geomagic Studio 2012 for model cleanup and noise reduction along with alignment and comparison of the photogrammetry and laser data; Zbrush v. 4R3 for further model cleanup and noise reduction.

Embryo remains were µCT scanned using the North Star Imaging µCT scanner of the Department of Earth and Environmental Sciences at Vanderbilt University (TN, USA). Voxel size ranged from 20.8 to 32.5 µm, beam voltage ranged from 77 to 121 kV. Volume was reconstructed using EFX-CT (North Star Imaging, Minnesota, USA). Scans were segmented using Object Research Systems application Dragonfly. We used R 4.0.5, Adobe Photoshop and Adobe Illustrator for data analysis and visualization.

Taphonomy and size distribution

Standard measurements (e.g. humerus proximodistal length, vertebra anteroposterior length and average diameter) were measured using measuring tapes or calipers, recorded to the nearest millimeter. Skeleton orientations in Quarry 2 were measured using a Brunton compass to determine the declination of the main body axis of each skeleton. When a skeleton was bent, or partially disarticulated, separate declinations were recorded for each segment. Photographs and 3D models were used to verify and build upon direct observations in the field. Additional data were compiled from published and unpublished sources including ref. 6 and original field notes and drawings archived at UCMP.

The taphonomic state (completeness and articulation, following ref. 20) of each specimen within Quarry 2 was assessed directly over the course of multiple visits to the site between 2014 and 2019. Additionally, a high-resolution digital model of the quarry was generated using laser scanning with a Faro Focus 3D and photogrammetry using digital SLR cameras (supplemental materials). This model was used to generate a high-resolution orthographic photomosaic of the quarry (Figure 2, Figure S1a) which in turn was used to create a detailed quarry map (Figure S1b-c). The digital model, orthographic photo and quarry map provided a complementary source of data for scoring the completeness and articulation state of each specimen within the quarry. Finally, these observations were compared with previous assessments[6,7,17,26.]

In addition to scoring the seven specimens preserved *in situ* within Quarry 2, we calculated approximate completeness and articulation scores for eleven additional specimens from six additional localities within the Luning Formation at West Union Canyon (Table S3). Ten of these specimens were specimens reported by Camp in his description of *Shonisaurus*[6] or his field notes, quarry maps and photographs obtained from the archives of the University of California Museum of Paleontology. The published and unpublished descriptions, diagrams and photographs were used to estimate completeness and articulation scores for these specimens (Figure S2). Five of these specimens are in collections at the Nevada State Museum, Las Vegas and one specimen is still visible in the park although it is exposed to the elements and its condition has likely deteriorated since its initial discovery. The current status of the other five specimens is unknown and they may have been lost or reburied. One additional new specimen (UMNH VP 32545) discovered during the course of our investigations in 2015 was excavated

and collected in 2016–2017. Although this specimen awaits complete preparation and study, its articulation and completeness were scored from photographs, field notes and quarry maps and included in this analysis.

Field investigation and Geological Methods

In addition to examination of *in situ* fossils in Quarry 2, we relocated three additional quarries (3, 5 and 6) and determined the approximate location of other original localities. We systematically searched all three members of the Luning Formation exposed in WUC for additional vertebrate fossils and recorded their location with handheld GPS receivers. We used existing geologic maps and stratigraphic sections as well as associated invertebrate fossils to determine the stratigraphic positions of these localities.

Fresh, unweathered outcrop was exposed at quarries 2, 5, and 6 to measure detailed stratigraphic sections and take lithologic samples. Each stratigraphic unit was measured using a Jacob's staff, correcting for dip of the beds, and was described in hand sample; in the case of carbonate layers, thin sections viewed in plane and cross-polarized light supplemented the field description. Samples for geochemical analysis were powdered from freshly exposed faces on these hand samples. To measure TOC and bulk $\delta^{13}C_{org}$, powdered samples were acidified and then analyzed using a Thermo Finnigan Delta Plus XL IRMS connected to a Carlo Erba Elemental Analyzer (EA, model 1010) via a Thermo Finnigan Conflo III at the Stable Isotope Ratio Facility for Environmental Research (SIRFER), University of Utah. To measure Hg concentration, untreated powdered samples were analyzed using RA-915 Portable Mercury Analyzer with PYRO-915 Pyrolyzer (Lumex) at the University of Oxford. A subset of untreated powdered samples were measured for TOC using Rock Eval VI analysis, also at the University of Oxford.

In the field, hand tools were used to expose (between ~30-150 cm below the surface) a continuous vertical profile of fresh, unweathered strata at Quarries 2, 5, and 6. The strike and dip of beds was measured using a Brunton Pocket Transit, and these values used to correct stratigraphic unit thickness measurements taken with a Precision Jacob's Staff (ASC Scientific). Each unit was described in fresh hand sample and characterized using a Munsell Rock Color Chart[55]. Carbonate layers were also described in thin section using a binocular petrographic microscope in both plane and cross-polarized light. Carbonate classification follows refs. 56 and 57, and the densities of clasts and fossils were estimated using charts from ref. 58. Unweathered samples were collected at 10-50 cm intervals from every unit for geochemical analysis.

Fresh surfaces on each sample were cleaned with deionized water, air-dried, and then powdered using a shatter box. To acidify the samples prior to analysis of total organic carbon content (TOC) and bulk $\delta^{13}C_{org}$ values, 10-15 ml was placed in a clean 100 ml beaker to which 60 ml of 1M HCl was added. Theses beakers were then placed in a 50°C water bath for 24 hours, after which the samples were filtered with deionized water using a vacuum pump and oven dried. Approximately 25 mg of each sample was weighed for $\delta^{13}C_{org}$ and TOC measurements made using a Thermo Finnigan Delta Plus XL IRMS connected to a Carlo Erba Elemental Analyzer (EA, model 1010) via a Thermo Finnigan Conflo III at the Stable Isotope Ratio Facility for Environmental Research (SIRFER), University of Utah. These analyses did not use He dilution, and raw data were normalized using three sets of internal lab reference materials (PLRM-1, PLRM-2, and SLRM) that are calibrated against USGS40 and USGS41.

A subset of untreated bulk powdered samples was also analyzed to determine TOC without acidification and characterize kerogen type and maturity, using a Rock-Eval VI at the

University of Oxford. TOC values were very low for all measured samples, with only one sample exceeding 0.2 wt%, with the low quantity of kerogen hindering robust interpretation of the other measured Rock-Eval parameters. The mercury concentrations of untreated bulk powdered samples were determined on a RA-915 Portable Mercury Analyzer with PYRO-915 Pyrolyzer (Lumex) at the University of Oxford, following the procedure outlined in ref. 60. Two aliquots of 50 ± 2 mg were measured to check reproducibility, which was better than ±10%, with NIST/UOE/FM/001 – Inorganic Elements in Peat (169 ppb Hg) utilized as a reference material to ensure machine accuracy. Hg concentrations show considerable variations throughout the stratigraphy at Quarry 2, ranging 2.6 to 139.5 ppb. The lithology is not suggestive of a strongly oxygen-depleted environment, nor do the Hg peaks show a clear correlation with lithological variations, suggesting that deposited mercury was not influenced by redox or lithology changes, and was primarily deposited with organic matter. However, interpretation of the Hg/TOC values is hindered by most samples featuring a TOC content below that recommended for mercury normalization[61]. Geochemical data are shown on Figure 1 and Figure S3 and reported in Table S2.

QUANTIFICATION AND STATISTICAL ANALYSES

Quantitative data presented in Figures 1–3, S3, Tables 1 and S1–3 were compiled and calculated in Microsoft Excel and R version 4.0.3. following the methods detailed above.

Methods S1. Descriptive, Taxonomic, Stratigraphic and Taxonomic Notes, related to Figures 1, 3, S3 and S4, Tables 1 and S2.

Supplementary Information is available for this paper.

Data availability statement

The µCT datasets generated by the current study are available at Morphosource (https://www.morphosource.org/) and 3D surface data at SI FigShare (https://smithsonian.figshare.com/). The 3D model is also catalogued in the collections of the Smithsonian National Museum of Natural History: http://n2t.net/ark:/65665/33ca0e041-4ae9-4b74-bfab-fd9885f2dffa. Fossil locality data are not publicly available, but kept on file at UMNH.

Correspondence and requests for materials should be addressed to Neil Kelley, neil.p.kelley@vanderbilt.edu

References

1. Veit, R.R., Silverman, E.D. and Everson, I. (1993). Aggregation patterns of pelagic predators and their principal prey, Antarctic krill, near South Georgia. J. Anim. Ecol. *62*, 551–564. 10.2307/5204
2. Benoit-Bird, K.J., Battaile, B.C. Heppell, S.A., Hoover, B., Irons, D., Jones, N., Kuletz, K.J., Nordstrom, C.A., Paredes, R., Suryan, R.M. et al. (2013). Prey patch patterns predict habitat use by top marine predators with diverse foraging strategies. PLoS ONE 8, e53348. 10.1371/journal.pone.0053348

3. Cassini, M.H. (1999). The evolution of reproductive systems in pinnipeds. Behav. Ecol. *10*, 612–616. 10.1093/beheco/10.5.612
4. Stokes, D.L. and Boersma, P.D. (2000). Nesting density and reproductive success in a colonial seabird, the Magellanic penguin. Ecology *81*, 2878–2891. 10.1890/0012-9658(2000)081[2878:NDARSI]2.0.CO;2
5. Yen, P.P.W., Sydeman, W.J. and Hyrenbach, K.D. (2004). Marine bird and cetacean associations with bathymetric habitats and shallow-water topographies: implications for trophic transfer and conservation. J. Mar. Syst. *50*, 79–99. 10.1016/j.jmarsys.2003.09.015
6. Camp, C.L. (1980). Large ichthyosaurs from the Upper Triassic of Nevada. Palaeontographica Abt. A *170*, 139–200.
7. Hogler, J.A. (1992). Taphonomy and paleoecology of *Shonisaurus popularis* (Reptilia: Ichthyosauria). Palaios *7*, 108–117. 10.2307/3514800
8. Block, B.A., Jonsen, I.D., Jorgensen, S.J., Winship, A.J., Shaffer, S.A., Bograd, S.J., Hazen, E.L., Foley, D.G., Breed, G.A., Harrison, A.L. and Ganong, J.E. (2011). Tracking apex marine predator movements in a dynamic ocean. Nature *475*, 86–90. 10.1038/nature10082
9. Piatt, J. and Methven, D. (1992). Threshold foraging behavior of baleen whales. Mar. Ecol. Prog. Ser. *84*, 205–210. http://www.jstor.org/stable/24829558
10. Norris, R.D., Turner, S.K., Hull, P.M. and Ridgwell, A. (2013). Marine ecosystem responses to Cenozoic global change. Science *341*, 492–498. 10.1126/science.1240543
11. Kidwell, S.M. (2015). Biology in the Anthropocene: challenges and insights from young fossil records. Proc. Natl. Acad. of Sci. *112*, 4922–4929. 10.1073/pnas.1403660112
12. Pyenson, N.D., Irmis, R.B., Lipps, J.H., Barnes, L.G., Mitchell, E.D. and McLeod S.A. (2009). Origin of a widespread marine bonebed deposited during the middle Miocene Climatic Optimum. Geology *37*, 519–522. 10.1130/G25509A.1
13. Delsett, L.L., Novis, L.K., Roberts, A.J., Koevoets, M.J., Hammer, Ø., Druckenmiller, P.S. and Hurum, J. (2016). The Slottsmøya marine reptile Lagerstätte: depositional environments, taphonomy and diagenesis. Geol. Soc. Spec. Pub. *434*, 165–188. 10.1144/SP434.2
14. Balini, M., Jenks, J.F., Martin, R., McRoberts, C.A., Orchard, M.J. and Silberling, N.J. (2015). The Carnian/Norian boundary succession at Berlin-Ichthyosaur State Park (Upper Triassic, central Nevada, USA). Palaontol. Z. *89*, 399–433. 10.1007/s12542-014-0244-2
15. Silberling, N.J. (1959). Pre-Tertiary stratigraphy and Upper Triassic paleontology of the Union District, Shoshone Mountains, Nevada. U.S. Geol. Surv. Prof. Pap. *322*, 1-67.
16. Buffrénil, V. de and Mazin, J.-M. (1990). Bone histology of the ichthyosaurs: comparative data and functional interpretation. Paleobiology *16*, 435–447. http://www.jstor.org/stable/2400968
17. McGowan, C. and Motani, R. (1999). A reinterpretation of the Upper Triassic ichthyosaur *Shonisaurus*. J. Vert. Paleontol. *19*, 42–49. 10.1080/02724634.1999.10011121
18. Dal Corso, J., Ruffell, A. and Preto, N. (2018). The Carnian Pluvial Episode (Late Triassic): new insights into this important time of global environmental and biological change. J. Geol. Soc. London *175*, 986–988. 10.1144/jgs2018-185
19. Greene, A.R., Scoates, J.S., Weis, D., Katvala, E.C., Israel, S. and Nixon, G.T. (2010). The architecture of oceanic plateaus revealed by the volcanic stratigraphy of the accreted Wrangellia oceanic plateau. Geosphere *6*, 47–73. 10.1130/GES00212.1
20. Mazaheri-Johari, M., Gianolla, P., Mather, T.A., Frieling, J., Chu, D. and Dal Corso, J. (2021). Mercury deposition in Western Tethys during the Carnian Pluvial Episode (Late Triassic). Sci. Rep. *11*, 17339. doi.org/10.1038/s41598-021-96890-8

21. Dickens, G.R., O'Neil, J.R., Rea, D.K. and Owen, R.M. (1995). Dissociation of oceanic methane hydrate as a cause of the carbon isotope excursion at the end of the Paleocene. Paleoceanography *10*, 965–971. 10.1029/95PA02087
22. Beardmore, S.R. and Furrer. H. (2016). Evidence of a preservational gradient in the skeletal taphonomy of Ichthyopterygia (Reptilia) from Europe. Palaeogeo. Palaeoclim. Palaeoecol. *443*, 131–144. 10.1016/j.palaeo.2015.11.049
23. Scheyer, T.M., Romano, C., Jenks, J. and Bucher, H. (2014). Early Triassic marine biotic recovery: the predators' perspective. PLoS ONE 9, e88987. 10.1371/journal.pone.0088987
24. Massare, J.A., Lomax, D.R. and Klein, A. (2015). A large forefin of *Ichthyosaurus* from the U.K., and estimates of the size range of the genus. Paludicola *10*, 119–135.
25. Klein, N., Schmitz, L., Wintrich, T. and Sander, P. M. (2020). A new cymbospondylid ichthyosaur (Ichthyosauria) from the Middle Triassic (Anisian) of the Augusta Mountains, Nevada, USA. J. Syst. Palaeontol. *18*, 1167–1191. 10.1080/14772019.2020.1748132
26. Kosch, B.F. (1990). A revision of the skeletal reconstruction of *Shonisaurus popularis* (Reptilia: Ichthyosauria). J. Vert. Paleontol. *10*, 512–514. 10.1080/02724634.1990.10011833
27. Stinnesbeck, W., Frey, E., Rivas, L., Pardo Pérez, J., Cartes, M.L., Soto, C.Z. and Lobos, P.Z. (2014). A Lower Cretaceous ichthyosaur graveyard in deep marine slope channel deposits at Torres del Paine National Park, southern Chile. Geol. Soc. Am. Bull. *126*, 1317–1339. 10.1130/B30964.1
28. Kear, B.P. (2006). Marine reptiles from the Lower Cretaceous of South Australia: elements of a high-latitude cold-water assemblage. Palaeontology *49*, 837–856. 10.1111/j.1475-4983.2006.00569.x
29. Maxwell, E.E. and Dececchi, T.A. (2013). Ontogenetic and stratigraphic influence on observed phenotypic integration in the limb skeleton of a fossil tetrapod. Paleobiology *39*, 123–134. 10.1666/0094-8373-39.1.123
30. Massare, J. A. (1987). Tooth morphology and prey preference of Mesozoic marine reptiles. J. of Vert. Paleontol. *7*, 121-137.
31. Nicholls, E.L. and Manabe, M. (2004). Giant ichthyosaurs of the Triassic—a new species of *Shonisaurus* from the Pardonet Formation (Norian: Late Triassic) of British Columbia. J. Vert. Paleontol. *24*, 838–849. 10.1671/0272-4634(2004)024[0838:GIOTTN]2.0.CO;2
32. Sander, P.M., Chen, X., Cheng, L. and Wang, X. (2011). Short-snouted toothless ichthyosaur from China suggests Late Triassic diversification of suction feeding ichthyosaurs. PLoS ONE 6, e19480. 10.1371/journal.pone.0019480
33. McGaughey, G., Noble, P., Kelley, N., Irmis, R. and dePolo, P. (2021). Hunting for the latest large-bodied ichthyosaur in the upper Triassic Luning Formation, Mineral County, Nevada, U.S.A. Geol. Soc. Am. Abst. with Prog. *53*, 11-1.
34. Stanley, G.D.J. (1979). Paleoecology, structure, and distribution of Triassic coral buildups in western North America. Univ. Kans. Paleontol. Contrib. *68*, 1–58.
35. Callaway, J.M. and Massare, J.A. (1989). *Shastasaurus altispinus* (Ichthyosauria, Shastasauridae) from the Upper Triassic of the El Antimonio district, northwestern Sonora, Mexico. J. Paleontol. *63*, 930–939.
36. McGowan, C. and Motani, R. Handbook of Paleoherpetology: Vol. 8 Ichthyopterygia. (2003) (Verl. Dr. Friedrich Pfeil, Munich).
37. Adams, T.L. (2009). Deposition and taphonomy of the Hound Island Late Triassic vertebrate fauna: fossil preservation within subaqueous gravity flows. Palaios *24*, 603–615. 10.2110/palo.2009.p09-010r

38. Slater, G.J., Goldbogen, J.A. and Pyenson, N.D. (2017). Independent evolution of baleen whale gigantism linked to Plio-Pleistocene ocean dynamics. Proc. Roy. Soc. B *284*, 20170546. 10.1098/rspb.2017.0546
39. Jenks, J.F., Monnet, C., Balini, M., Brayard, A. and Meier, M. (2015) Biostratigraphy of Triassic ammonoids. In Ammonoid Paleobiology: From Macroevolution to Paleogeography. (Springer, Dordrecht), pp. 329–388.
40. Motani, R., Jiang, D. Y., Tintori, A., Rieppel, O. and Chen, G. B. (2014). Terrestrial origin of viviparity in Mesozoic marine reptiles indicated by Early Triassic embryonic fossils. PLoS ONE *9*, e88640. 10.1371/journal.pone.0088640
41. Maxwell, E.E. and Caldwell, M.W. (2003). First record of live birth in Cretaceous ichthyosaurs: closing an 80 million year gap. Proc. Roy. Soc. B *270*. 10.1098/rsbl.2003.0029
42. Deeming, D., Halstead, L., Manabe, M. and Unwin, D.M. (1993). An ichthyosaur embryo from the Lower Lias (Jurassic: Hettingan) of Somerset, England, with comments on the reproductive biology of ichthyosaurs. Modern Geology 18, 423–442.
43. Corkeron, P.J. and Connor, R.C. (1999). Why do baleen whales migrate? Mar. Mamm. Sci. *15*, 1228–1245.
44. Clapham, P. (2001). Why do baleen whales migrate? Mar. Mamm. Sci 17, 432–436.
45. Vermeij, G.J. (1977). The Mesozoic marine revolution: evidence from snails, predators and grazers. Paleobiology *3*, 245–258.
46. Knoll, A.H. and Follows, M.J. (2016). A bottom-up perspective on ecosystem change in Mesozoic oceans. Proc. Roy. Soc. B *283*, 20161755. 10.1098/rspb.2016.1755
47. Fröbisch, N.B., Fröbisch, J., Sander, P.M., Schmitz, L. and Rieppel, O. (2013). Macropredatory ichthyosaur from the Middle Triassic and the origin of modern trophic networks. Proc. Natl. Acad. of Sci. *110*, 1393–1397. 10.1073/pnas.1216750110
48. Sander, P.M. et al. (2021). Early giant reveals faster evolution of large body size in ichthyosaurs than in cetaceans. Science 374. 10.1126/science.abf5787
49. Kelley, N.P. and Pyenson, N.D. (2015). Evolutionary innovation and ecology in marine tetrapods from the Triassic to the Anthropocene. Science *348*. 10.1126/science.aaa3
50. Massare, J.A. (1988). Swimming capabilities of Mesozoic marine reptiles: implications for method of predation. Paleobiology *14*, 187–205.
51. Motani, R., Rothschild, B. M. and Wahl, W. (1999). Large eyeballs in diving ichthyosaurs. Nature *402*, 747.
52. Fischer, V., Arkhangelsky, M. S., Uspensky, G. N., Stenshin, I. M., and Godefroit, P. (2014). A new Lower Cretaceous ichthyosaur from Russia reveals skull shape conservatism within Ophthalmosaurinae. Geol. Mag. *151*, 60-70. 10.1017/S0016756812000994
53. Oliver, J., Slattery, P., Silberstein, M. and O'Connor, E. (1983). A comparison of gray whale, *Eschrichtius robustus*, feeding in the Bering Sea and Baja California. Fish. Bull. (Wash. D.C.) *81*, 513–522.
54. Martindale, R.C., Corsetti, F. A., James, N. P. and Bottjer, D. J. (2015). Paleogeographic trends in Late Triassic reef ecology from northeastern Panthalassa. Earth-Sci. Rev. *142*, 18–37. 10.1016/j.earscirev.2014.12.004
55. Geological Society of America (1991). Rock-Color Chart. (Geological Society of America, Boulder)
56. Folk, R.L. (1959). Practical petrographic classification of limestones. Am. Assoc. Pet. Geol. Bull. *43*, 1–38.

57. Dunham, R.J. Classification of carbonate rocks according to depositional texture. (1962) AAPG Mem. *1*, 108–121.
58. Baccelle, L., and Bosellini, A. (1965). Diagrammi per la stima visiva della composizione percentuale nelle roccē sedimentarie. Annali dell'Università degli di Ferrara, Sezione IX, Scienze Geologiche e Paleontologiche *4*, 59-62.
59. Behar, F., Beaumont, V., and Penteado, H.D.B. (2001). Rock-Eval 6 technology: performances and developments. Oil Gas Sci. Technol. *56*, 111–134.
60. Percival, L. M., Ruhl, M., Hesselbo, S.P., Jenkyns, H.C., Mather, T.M. and Whiteside, J.H. (2017). Mercury evidence for pulsed volcanism during the end-Triassic mass extinction. Proc. Natl. Acad. of Sci. *114*, 7929–7934. 10.1073/pnas.1705378114
61. Grasby, S.E., Beauchamp, B., Bond, D.P.G., Wignall, P. and Sanei, H., (2015). Mercury anomalies associated with three extinction events (Capitanian crisis, latest Permian extinction and the Smithian/Spathian extinction) in NW Pangea. Geol. Mag. *153*, 285–297. 10.1017/S0016756815000436

Table 1. West Union Canyon vertebrate fossil specimens by ammonoid zone and taphonomic state.

Taxon	Ammonoid horizon	Taphonomic State		
		Isolated	Associated	Semi-Articulated
Shonisaurus sp.	*S. kerri*	1	1	
	K. macrolobatus	8	59	9
	K. schucherti	2	1	
Ichthyosauria indet. (cf. *Shonisaurus sp.)*	*K. macrolobatus*	19	5	
	K. schucherti	3		
Other Vertebrates				
Chondrichthyes	*K. macrolobatus*	1		
Actinopterygii	*S. kerri*	1		
Vertebrata Indet.	*S. kerri* (or above)	2		

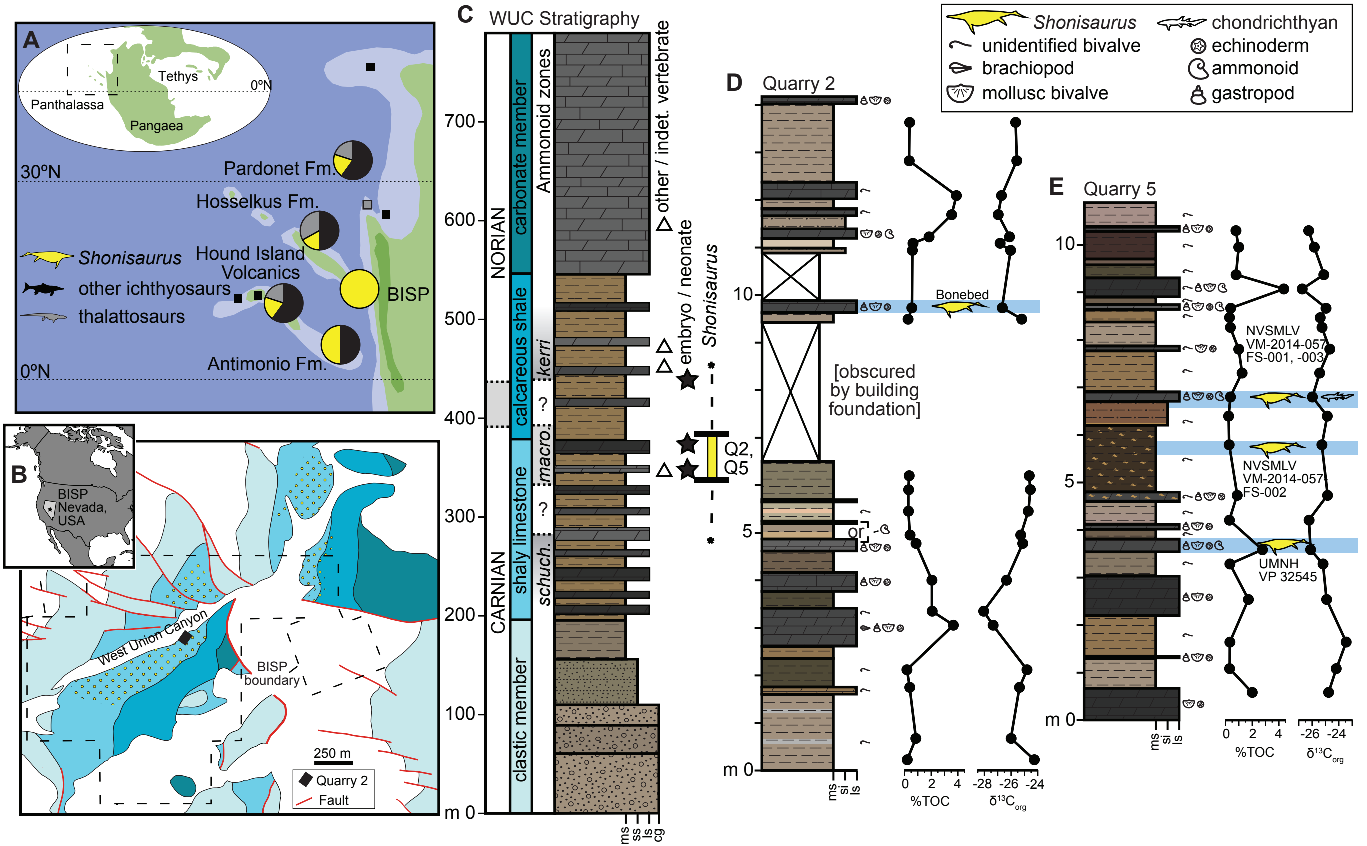
A
Tethys
0ºN
Panthalassa
Pangaea
30ºN
Pardonet Fm.
Hosselkus Fm.
Hound Island Volcanics
Shonisaurus
other ichthyosaurs
thalattosaurs
BISP
0ºN
Antimonio Fm.
B
BISP Nevada, USA
West Union Canyon
BISP boundary
250 m
Quarry 2
Fault
C
WUC Stratigraphy
NORIAN
CARNIAN
carbonate member
calcareous shale
shaly limestone
clastic member
Ammonoid zones
kerri
macro.
schuch.
?
other / indet. vertebrate
embryo / neonate
Shonisaurus
Q2, Q5
700
600
500
400
300
200
100
m 0
ms ss ls cg
D
Quarry 2
Bonebed
[obscured by building foundation]
or
10
5
m 0
ms si ls
%TOC
δ13Corg
E
Quarry 5
NVSMLV VM-2014-057 FS-001, -003
NVSMLV VM-2014-057 FS-002
UMNH VP 32545
10
5
m 0
ms si ls
%TOC
δ13Corg
Shonisaurus
unidentified bivalve
brachiopod
mollusc bivalve
chondrichthyan
echinoderm
ammonoid
gastropod

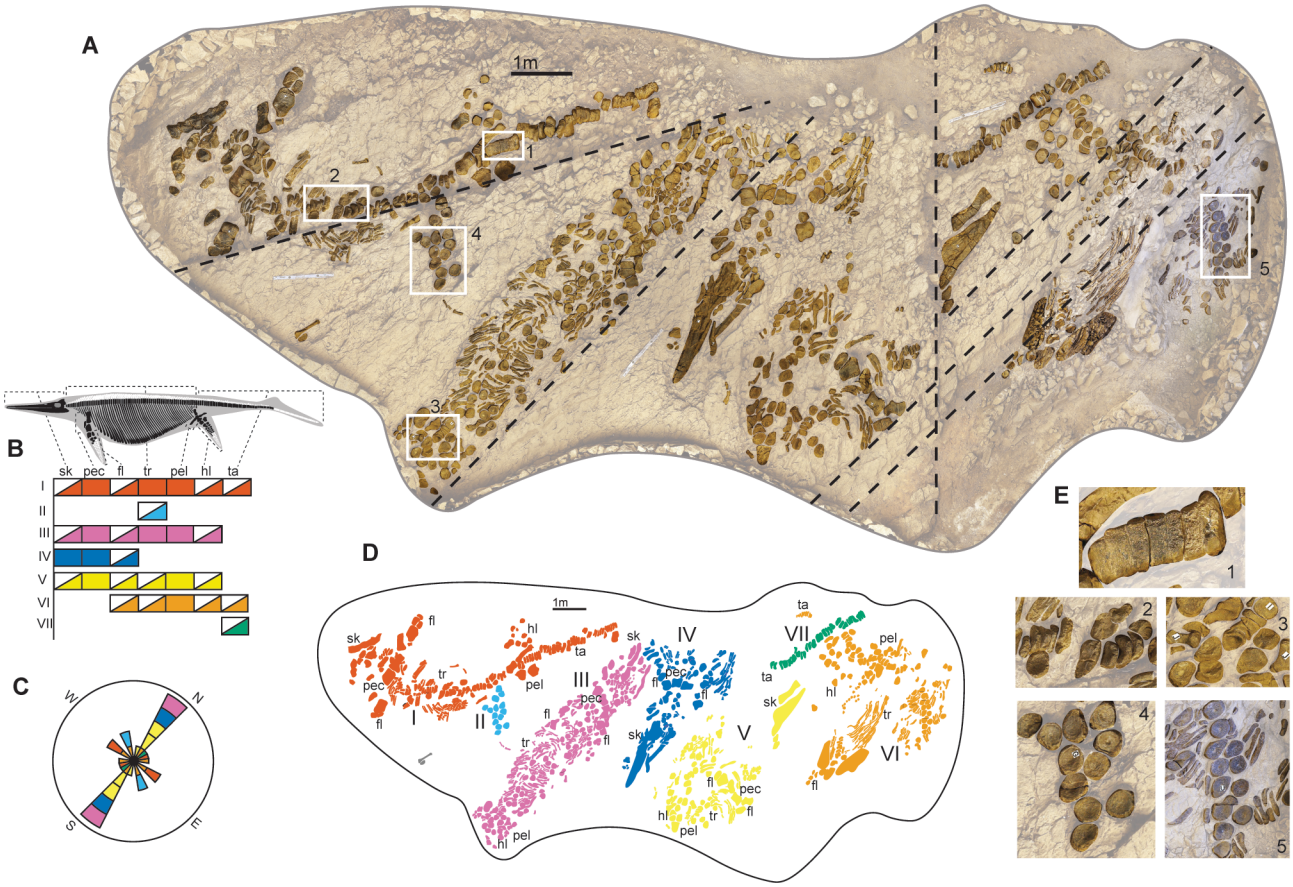
A
1m
1
2
3
4
5
B
sk
pec
fl
tr
pel
hl
ta
I
II
III
IV
V
VI
VII
C
W
N
S
E
D
1m
E
1
2
3
4
5

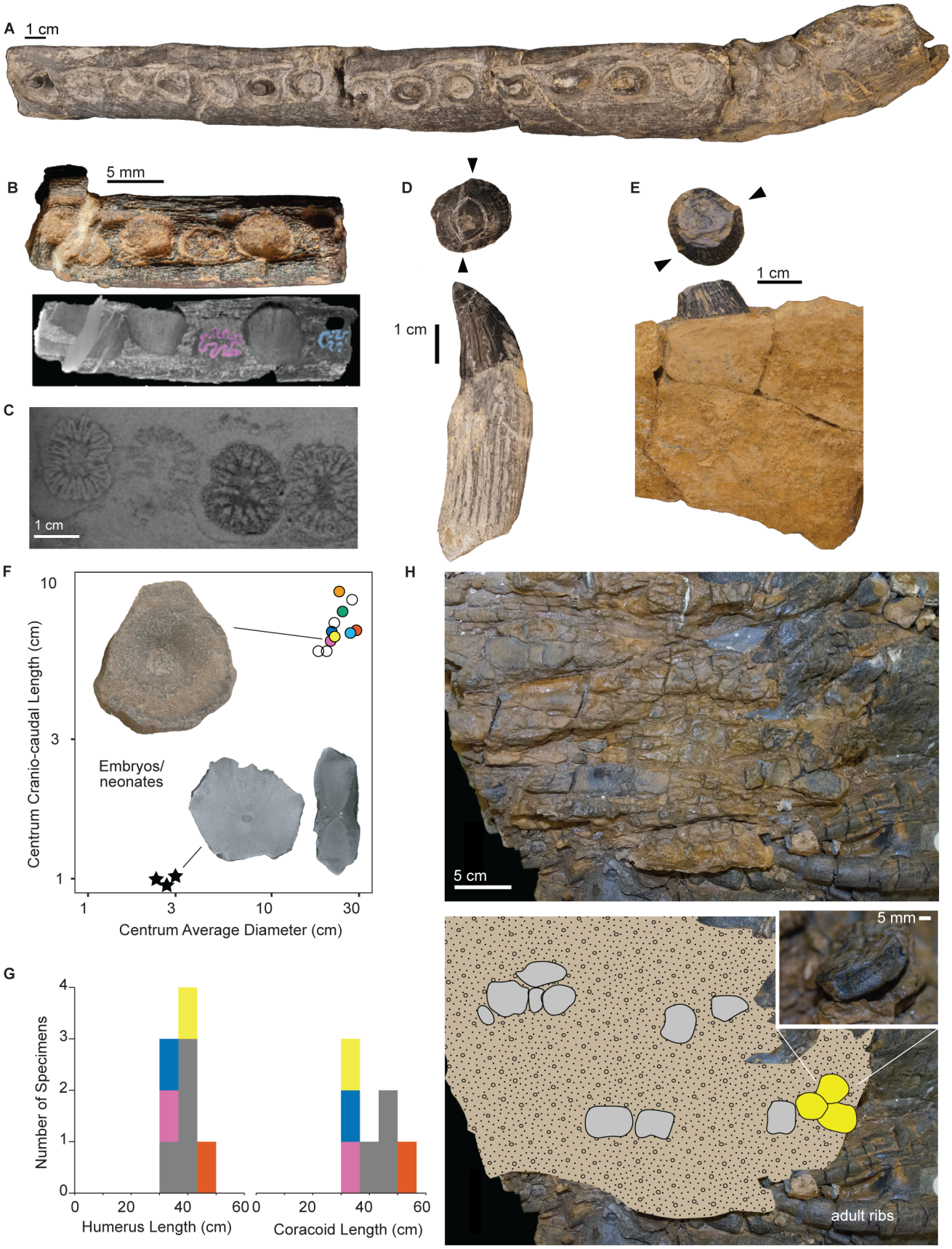
A
1 cm
B
5 mm
C
1 cm
D
1 cm
E
1 cm
F
Centrum Cranio-caudal Length (cm)
10
3
1
Embryos/
neonates
1
3
10
30
Centrum Average Diameter (cm)
G
Number of Specimens
4
3
2
1
0
0
20
40
60
Humerus Length (cm)
0
20
40
60
Coracoid Length (cm)
H
5 cm
5 mm
adult ribs

Methods S1

Description of *Shonisaurus* embryonic remains

The majority of *Shonisaurus* occurrences in WUC represent large, skeletally mature individuals, though we note three discrete occurrences representing embryonic or neonatal individuals. NSMLV VM-2014-057-FS-001 (Figures 3f, h; S5d, e) comprises a mass of small bones within the posterior abdomen of the type specimen. This material was alluded to by Camp (ref. S1 and unpublished field notes) but never figured or described in detail. The majority of elements are disarticulated vertebral centra, while others may represent limb or girdle elements as well as fragmentary ribs, however these latter are obscured by matrix and epoxy used to stabilize the fossil and require further preparation or µCT scanning for confident identification. Camp's unpublished field notes also mention an "embryonic skull" but the current whereabouts of this material is unknown. Three vertebral centra, each approximately 2.5-3.5 cm in diameter and 1 cm in antero-posterior length, were removed for µCT scanning. Despite being partially obscured by matrix, x-ray imagery revealed shape, proportion and bone texture consistent with the identification of these elements as extremely small *Shonisaurus* vertebra, showing the same high centrum diameter to length ratio of approximately three[S8] (Table S1). Centra are deeply amphicoelous, with an open notochordal foramen. A distinctive cruciform ossification pattern resembles that reported for other embryonic ichthyosaur centra[S9] and may reflect their early developmental stage. No evidence of maceration or etching by digestive acids is observed and given their close resemblance to the vertebral morphology of *Shonisaurus* and their placement in the pelvic region of the type specimen these remains are regarded as *in situ* embryos, rather than gut contents. We regard the disarticulation of the embryonic remains to reflect postmortem decomposition and collapse and compression of the adult skeleton before and during burial.

Another small centrum, VM-2014-057-FS-007, found loose in associated collections, was scanned and revealed identical morphology to the *in situ* specimens (Figure S5b).

A very small (approximately 2.25 cm diameter, 1 cm in antero-posterior length) surface-collected, isolated vertebral centrum, UMNH VP 32547 (Figure S5c), found in a different region of the canyon is a close match with those found *in situ* within the type specimen being similar in size and retaining an open notochordal canal. A surface-collected fragmentary jaw (UCMP 290269), from yet another location, was identified in a museum collection of invertebrate specimens collected during the 1990s. This specimen shows a close resemblance with the dentigerous jaw of *Shonisaurus,* bearing teeth with highly infolded roots set in distinct sockets, but is only 2.7 cm long and 0.6 cm in transverse width. This jaw fragment exhibits five alveoli averaging 0.4 cm in diameter separated by thin bony partitions. Two alveoli are occupied by partial teeth with heavily plicated roots (Figures 3, S5a). Although incomplete, both root shape and implantation in sockets closely resembles the condition observed in *Shonisaurus*[S1]. A prominent neurovascular canal occupies twenty percent of the cross-sectional width of the jaw and contains a mineralized structure, likely a preserved remnant of the Meckelian cartilage (Figures 3, S4 A).

Taxonomic status of *Shonisaurus* and referred material.

Three species of *Shonisaurus* were originally described from WUC[S1] namely, *S. popularis, S. silberlingi* and *S. mulleri.* However, these were later synonymized into a single species, *S. popularis*[S8] Personal observation of the type material of the three species, along with the *in situ* specimens in Quarry 2 and additional material collected during the present study, confirms notable differences, primarily in humeral morphology, among specimens. Whether these differences represent distinct species, or individual, ontogentic or sexual variation is

beyond the scope of the current study. The original three nominal species occur on different horizons within Luning Formation exposures in WUC, raising the possibility that they represent chronospecies. Until a detailed comparison can be made, we provisionally accept that all *Shonisaurus* remains at WUC can be referred to a single species, *S. popularis.*

A second valid species referred to *Shonsiaurus* is *S. sikanniensis* from the Norian aged Pardonet Formation of British Columbia[S10]. Although larger, this species resembles *Shonisaurus popularis* in several respects including vertebrae with a relatively high diameter to length ratio (though not as high as *S. popularis*), robust ribs with a pronounced distal expansion, proximally expanded coracoid and a robust subrectangular humerus. Juveniles of *S. sikanniensis* are reported to possess teeth set in individual sockets, as with *S. popularis*, although adults are reportedly edentulous—this is *not* the case for *S. popularis* contra ref. S10. While some phylogenetic analyses have found *S. sikanniensis* and *S. popularis* to be sister taxa[S11], consistent with their congeneric status, others do not find them to be closely related[S12] and some have suggested *S. sikannensis* should be referred to the related but distinct genus *Shastasaurus*[S13].

The genus *Shonisaurus* has been reported from a number of additional Triassic-aged localities in western North America[S1,S14–S16], however much of this material is fragmentary and most of these remains have only been assigned to *Shonisaurus* sp. Fragmentary remains of large ichthyosaurs with some resemblance to *Shonisaurus* have also been reported from Europe[S17,S18], Tibet[S19] and Australasia[S20].

Stratigraphic distribution of *Shonisaurus* at West Union Canyon.

Ichthyosaur fossils were first discovered in the Luning Formation of West Union Canyon (WUC), Nye County, Nevada in the 1930s but were not excavated until the 1950s[S1]. The original excavations revealed more than thirty specimens all belonging to a single genus of giant

ichthyosaur, *Shonisaurus*. These specimens were distributed across at least ten separate localities spanning two kilometers of WUC (Figures 1, S2, Table S4). The most significant localities were designated quarry numbers by Camp including Quarry 2, now preserved as an *in situ* fossil display and Quarry 5 where the type material was collected. Ichthyosaur fossils are primarily concentrated within the shaly limestone member, in the *Klamathites macrolobatus* ammonoid zone[15] although fragmentary remains have also been reported from the underlying *K. schucherti* zone in the lower portion of the shaly limestone member. Both of these ammonoid zones are regarded as late Carnian in age. Hogler (ref. S2) suggested that ichthyosaur fossils in WUC Luning Formation exposures extended over a broader stratigraphic interval, with a 'scattered element' taphofacies extending 200 meters below and 400 meters above a 200-meter-thick 'articulated skeleton' taphofacies, although this extension was recently questioned[S21]. Our results confirm that *Shonisaurus* fossils are most abundant in the *K. macrolobatus* portion of the shaly limestone member but extend down into the *K. schucherti* zone of that member and into the *K. macrolobatus* zone of the overlying calcareous shale member and two specimens were found within the lowermost *S. kerri* zone of the calcareous shale member (Table 1). We also relocated an indeterminate vertebrate fossil within the carbonate member previously reported by one of the authors[S22]. The spongy texture of this specimen is consistent with an ichthyosaurian identity but it is too incomplete for unambiguous identification.

Additional specimens referred to *Shonisaurus* have been reported from Luning Formation exposures about 70 km to the southwest, in the Pilot Mountain Range of Mineral County, Nevada[S1]. Recent field work by the authors confirms these reports.

Estimated duration of the *Klamathites macrolobatus* ammonoid zone

The *K. macrolobatus* zone correlates with the Tethyan *Anatropites spinosus* ammonoid biozone[S21,S23]; though no precise radioisotopic ages are available for this interval, there are magnetostratigraphic records from a number of sites[S24–SS7]. The *A. spinosus* biozone corresponds to the magnetic polarity zones PM1-PM4 at Pizzo Mondello in Sicily[S26,S29], and SB1-SB3 at Silickà Brezovà in Slovakia[S25]. These polarity zones correlate to E5n.1r-E7 of the astronomically-tuned Newark-Hartford astrochronostratigraphic polarity time-scale[S28], which is 230.1 to 226.8 Ma in age. This age range is also consistent with a high-resolution U-Pb zircon age of 230.91 ± 0.33 Ma from strata in southern Italy underlying the *spinosus* zone[S23–S30]. Thus, a maximum age duration estimate for the *macrolobatus* zone at BISP is ~3.3 million years.

No geochemical evidence for environmental perturbations

Mercury concentrations have been used by several studies to document increases in large igneous province volcanic activity (see reviews in refs. S31 and S32). However, it cannot be unambiguously stated whether the sedimentary Hg enrichments recorded at Quarry 2 document volcanic eruptions or not. Radioisotopic dating of rocks from the Wrangellian LIP, and osmium-isotope evidence of enhanced magmatism indicate that it formed during the Carnian Stage[S33,S34]. It should be noted that the main pulse of volcanic activity likely began during the latest Ladinian–earliest Carnian and concluded during the early Carnian[S35], significantly prior to the time interval when the *Shonisaurus*-rich strata formed, although the destruction of almost all Triassic oceanic crust means that a continuation of Wrangellian volcanism into the later Carnian cannot be completely ruled out. Crucially however, the main *Shonisaurus* bed at Quarry 2 features one of the lowest Hg concentrations of any stratigraphic layer measured from that site, suggesting that the ichthyosaur deaths did not coincide with a major influx of mercury to that area, whether volcanically sourced or otherwise. It should be noted that Wrangellia LIP was an

oceanic plateau, and studies of similar Cretaceous LIPs have highlighted that submarine volcanism on such provinces can have a limited influence on global mercury cycling[S36–38]. However, it is known that there were subaerial eruptions associated with the Wrangellia LIP, and Carnian mercury enrichments have been documented from Tethyan sites[S39], which were significantly further from Wrangellian volcanism than Quarry 2, although distribution of any submarine Hg emissions may have been influenced by the direction of oceanic currents rather than mere distance from source.

Moreover, the *Shonisaurus* bed at Quarry 2 does not correlate with the most prominent $\delta^{13}C$ excursion in recorded at that site, which is significantly stratigraphically lower, and may be associated with a change in the type of organic matter being deposited. Alternatively, the $\delta^{13}C$ values could reflect disrupted primary productivity or a flux of isotopically light carbon to the ocean-atmosphere system[S40,S41]. However, there is no evidence for a local perturbation in productivity, and global-scale $\delta^{13}C$ excursions that might support increased carbon emissions to the ocean/atmosphere are not known from late Carnian records. Thus, there is no positive geochemical evidence from either carbon isotopes or mercury concentrations that the abrupt burial and preservation of *Shonisaurus* was the result of volcanism, carbon-cycle perturbations, or environmental degradation.

Stratigraphic sections

Written descriptions of stratigraphic sections shown on Figure 1 and Figure S3. Representative thin sections are shown in Figure S4.

Quarry 2

At this outcrop, strata dip 10° to the east; strike of 160°.

Unit 1: 1.65 m – greyish pink (5R 8/2) crystalline rock with granular texture and oxide veins and zones of pale reddish brown (10R 5/4). In hand sample, black opaque cubic crystals are also visible (.5-1 mm diameter). Unit is massive with many diagonal fractures.

Thin section: Dominated by feathery crystalline quartz, with patches of variably-sized crystals of sparry calcite. Common but localized blotchy patches of dark brown opaque mineral. Widespread cubic to rhombohedral opaque (black) mineral that looks very dark red at high magnification. Sometimes these crystals have thin rims of small monocrystalline quartz crystals. Occasional long laminar crystals of ?mica. Occasional thin fractures lined by the blotchy opaque mineral and filled by sparry calcite.

Note: this unit was excluded from the figured stratigraphic column because it appears to be highly altered and the original lithology is not clear.

Unit 2: 1.60 m – pale yellowish brown (10YR 6/2) mudstone with zones of light grey (N7). Occasional flattened oval dolomitic concretions that are dark grey (N7). Some small oxidized burrows (~1 mm diameter) and poorly preserved molds of unidentified bivalves ~.6 m above the base of the unit.

Unit 3: 0.15 m – moderate yellowish brown (10YR 5/4) dolomite. Pervasive thin (0.5 mm) fractures filled by calcite spar.

Thin section: Approximately 50% siliciclastic mud, 50% small ?dolomite spar crystals, but proportion does vary throughout the section (stratigraphically up and down). Widespread small round opaque crystals similar to the blotchy mineral in Unit 1, but smaller and not as patchy. Rare rounded quartz fine sand grains (<1%) and very rare (<<1%) fossils that are completely recrystallized into monocrystalline calcite spar.

Abundant fractures sub-parallel and sub-perpendicular to bedding; these are filled by sparry ?calcite.

Unit 4: 0.60 m – olive grey (5Y 3/2) mudstone, not calcareous. Some small (~1 mm) unidentified bivalve fossils.

Unit 5: 0.25 m – highly weathered unit, probably same as Unit 4? Moderate yellowish brown (10YR 5/4) mudstone.

Unit 6: 0.80 m – dark grey (N3) dolomite with white (N9) veins of dolomite spar, 1-5 mm thick. This unit is massive with no bedding planes observed, and also fractured. Unidentified bivalves present in the upper 10 cm of the unit. Bivalve specimen preserved as UMNH IP 7003.

Thin section: Micrite matrix that has been recrystallized into microspar, with 25-30% skeletal grains (fossils). Most skeletal grains are recrystallized into spar, and some have dark brown mud fill. A couple skeletal grains are the core of peloids, and there are a number of skeletal grains that form the core of recrystallized oncoids; both have clear thin dark boundaries. Skeletal grains are poorly sorted; bivalves are disarticulated, often broken, and often at a high angle to bedding (both convex up and convex down). Skeletal grains include gastropods, bivalves, ?brachiopods, and echinoderms. A single ornamented shell might be a brachiopod. There are a few ~.5 mm multi-chambered skeletal grains that might be foraminifera, but its difficult to tell; they could also be oblique views of small gastropods. Occasional very small crystals of an opaque mineral. Pervasive spar-filled fractures at a high angle to bedding. A few highly recrystallized areas have stylolitic borders that are sub-perpendicular to bedding. Sparse biomicrite/packstone.

Unit 7: 0.35 m – olive grey (5Y 3/2) slightly calcareous mudstone. Deeply weathered and modern roots are found throughout.

Unit 8: 0.40 m – dark grey (N3) limestone, less dolomitized than other carbonate units. White dolomite spar veins similar to Unit 6.

Thin section: Micrite matrix recrystallized into microspar; these spar crystals are a little larger than in Unit 6. 10-15% skeletal grains, some of which are recrystallized, and some of which retain original structure. Poorly sorted skeletal grains; bivalves are disarticulated and tend to be broken, and oriented at various angles to bedding. Occasional dark brown mud-filled gastropods and rounded clasts of mud that contains a few spar crystals (peloids?). Skeletal grains include bivalves, gastropods, and echinoderms. Very pervasive fractures, mostly close to perpendicular to bedding, some have stylolitic borders. Fossiliferous to sparse micrite/mudstone to wackestone.

Unit 9: 0.45 m – dark yellowish brown (10YR 4/2) mudstone. Pervasive modern roots.

Unit 10: 0.25 m – medium dark grey (N4) dolomite. Massive; no visible bedding. Specimen of cf. *Tropites* sp. (UMNH IP 7004) found in trench is from either this horizon or Unit 12.

Thin section: Micrite matrix that is recrystallized into very small microspar crystals (like Unit 6), with ~15-20% skeletal grains. Most skeletal grains are recrystallized into spar, and include bivalves, gastropods, and echinoderms. Skeletal grains often infilled by even smaller microspar than matrix. Poorly sorted skeletal grains, but dominated by grains smaller than .5 mm. Bivalves are disarticulated and tend to be broken, but are generally sub-parallel to bedding. Abundant very small crystals of opaque minerals that are sometimes slightly dark red; shape varies from rounded to sub-

rectangular. Fractures still present throughout and sub-perpendicular to bedding, but less common than in Units 3, 6, 8. Sparse biomicrite/wackestone.

Unit 11: 0.32 m – greyish orange (10YR 7/4) to pale yellowish brown (10YR 6/2) calcareous mudstone.

Unit 12: 0.05 m – dark grey (N3) dolomite with white spar-filled fractures. Specimen of cf. *Tropites* sp. (UMNH IP 7004) found in trench is from either this horizon or Unit 10.

Unit 13: 0.40 m – mottled moderate orange pink (5YR 8/4) and yellowish grey (5Y 7/2) moderately calcareous mudstone with faint wispy laminations. Small fragments of shell are visible with hand lens.

Unit 14: 0.05 m – dark grey (N3) dolomite with white spar filling fractures. Appears to be altered and contain possible dissolution features.

Unit 15: 0.80 m – light olive grey (5Y 5/2) moderately calcareous mudstone.

Unit 16: 2.93 m – COVERED. [NW wall of quarry shelter]

Unit 17: 0.20 m – pale yellowish brown (10YR 6/2) slightly calcareous mudstone, breaks into tabular pieces, but no visible laminations or clear bedding planes.

Unit 18*: 0.20 to 0.30 m – Dark grey (N3) dolomite, massive with no clear bedding. Contains fractures 1-2 cm wide filled by white dolomite spar. Sparse invertebrate fossils visible in hand sample. Bones are very large but appear to be in the middle and upper part of the unit. ***Bonebed.***

Thin section: ~40% skeletal grains; some layers preserve original dark brown micrite, whereas others are recrystallized into variously-sized spar. Most skeletal grains are *not* recrystallized - some are infilled with microspar, whereas others are infilled with dark brown micrite mud. Overall it is poorly sorted, but most bivalves are in a similar

size class (2-3 mm long). Skeletal grains dominated by bivalves (mostly sub-parallel to bedding), but also include abundant gastropods and some echinoderms. Bivalves are disarticulated, some are complete, some broken, and both convex up and convex down. Just a few spar-filled fractures both sub-parallel and sub-perpendicular to bedding. Sparse biomicrite/packstone.

Exposed bonebed expresses numerous small faults with 10-50 cm of offset (see main text Figure 2), so this should be taken into consideration when assessing the accuracy of this measured section.

Unit 19: 1.0 m – COVERED. [SE wall of quarry shelter]

Unit 20: 0.10 m – Pale yellowish brown (10YR 6/2) moderately calcareous siltstone, breaks into tabular pieces, but no visible bedding planes.

Unit 21: 0.20 m – very pale orange (10YR 8/2) moderately calcareous mudstone, weakly laminated.

Unit 22: 0.20 m – dark grey (N3) dolomite with 1-2 mm wide fractures filled by dolomite spar. In situ specimen of Ammonoidea indet. (UMNH IP 7005) 10 cm above base of unit.

Thin section: Spar matrix, probably originally micrite, but a bit larger crystals than in previous units. ~10-20% skeletal grains, mostly recrystallized disarticulated bivalves, though there are a few echinoderm elements. Most shell pieces are broken and sub-perpendicular to bedding. Poorly sorted skeletal grains. There appears to be a vertical burrow-like structure that is filled with micrite towards the bottom, and spar towards the top. The structure also includes small bivalve shells, which are recrystallized in the spar, but it's difficult to tell their condition in the micrite. A few spar-filled cracks both sub-perpendicular and sub-parallel to bedding, one of which has stylolitic borders

for part of its length. Folk classification depends on whether the spar matrix is primary; it is either a sparse biomicrite or unsorted biosparite. If original matrix was micrite, Dunham classification is wackestone.

Unit 23: 0.27 m – pale yellowish brown (10YR 6/2) siltstone, not calcareous. Highly fractured with veins of dolomite spar.

Unit 24: 0.15 m – dark grey (N3) dolomite; spar-filled fractures are present, but less apparent than in other units.

Thin section: Microspar matrix with some interstitial original micrite. Skeletal grains very rare (<<1%), with only 2-3 recrystallized small disarticulated broken bivalves that are sub-perpendicular to bedding. Pervasive fine spar-filled fractures that are mostly sub-perpendicular to or 45-60° to bedding. Micrite/mudstone.

Unit 25: 0.20 m – pale yellowish brown (10YR 6/2) moderately calcareous mudstone, weakly laminated. Unit is deeply weathered.

Unit 26: 0.35 m – dark grey (N3) limestone; dolomite spar-filled fractures from .1 mm to 1 cm wide are present, but not common.

Thin section: Microspar matrix with some interstitial original micrite (similar to Unit 24). Skeletal grains are rare (1-5%; high end of that is localized), all are small broken disarticulated bivalves that are sub-perpendicular to bedding or otherwise at a high angle to bedding. There appear to be a few elliptically-shaped peloids, but they have irregular borders – possibly from the recrystallized spar crystals surrounding them. Very pervasive extremely fine spar-filled fractures, most of which are sub-parallel to bedding. Fossiliferous micrite/mudstone.

Unit 27: 1.65 m – Pale yellowish brown (10YR 6/2) mudstone, weakly laminated. Slightly concave bedding planes are weakly expressed. 2-5 cm carbonate-rich, more resistant beds present in unit. At ~ 1.1 m above the base of the unit, there is a sub-horizontal 2-3 cm thick dolomite spar vein.

Unit 28: 0.15 m – dark grey (N3) dolomite with many moderate red (5R 5/4) zones that appear to be altered and contain fracture planes.

Thin section: Matrix is ~50% micrite and ~50% very small microspar, with slightly higher proportions of micrite in the darker areas of the rock. ~20-30% skeletal grains, nearly all of which are recrystallized; they are sub-parallel to bedding and mostly concave up. Bivalves are most abundant, but gastropods and echinoderms are not uncommon. Skeletal grains are poorly sorted. Bivalves are disarticulated and mostly broken. A few cubic opaque minerals that are dark red at high magnification. Very pervasive spar-filled fractures that are mostly sub-perpendicular and sub-parallel to bedding, but also at other angles. Sparse biomicrite/wackestone.

Quarry 5

At this outcrop, strata dip 21° to the east; strike of 38°.

Unit 1: 0.67 m – greyish black (N2) dolomite with very fine (<1 mm) spar-filled fractures. Many of these fractures imitate bedding planes, but are actually perpendicular to bedding. Unit is massive, with no fossils visible in hand sample.

Thin section: Micrite matrix with wispy dark zones, and ~5% skeletal grains (fossils), except the top tenth of the thin sections where skeletal grain abundance is 10-

15% (Baccelle & Bosellini 1965). Most retain their original internal structure, though some larger bivalves are recrystallized. Skeletal grains include mollusc bivalves and echinoderms. Broken single valves of mollusc bivalves parallel/sub-parallel to bedding are the most common skeletal grain, though there are a few articulated bivalves. Some parts of the thin section have wispy/cloudy zones of spar that gradually merge into the micrite, and sometimes almost have a stylolitic shape, but at high angle to bedding. Occasional very thin vertical to sub-vertical spar-filled fractures. Fossiliferous micrite/mudstone.

Unit 2: 0.62 m – pale yellowish brown (10YR 6/2) calcareous mudstone. No apparent bedding planes, and breaks into blocky chunks.

Unit 3: 0.03 m – dark grey (N3) dolomite with angled fractures but none appear to be spar-filled (at least in hand sample).

Thin section: The entire sample shows variation from micrite to tiny microspar. The upper quarter and very bottom of the thin section contain 20-30% skeletal grains. About half of the skeletal grains are recrystallized, and about half of the small gastropods are filled by dark brown mud (no spar). Skeletal grains include mollusc bivalves, gastropods, and echinoderms, with the bivalves and gastropods by far the most common. Some smaller bivalves are articulated, but single valves of all sizes are more abundant. Skeletal grains show no preferred orientation. The grain size distribution is bimodal, with some large mollusc bivalves, but the gastropods, echinoderms and smaller bivalves in a single size class. This part of the thin section and the zone immediately below it contain abundant crystals of an opaque/very dark red mineral that are sometimes cubic/rhombic. Sparse biomicrite/wackestone. The rest of the thin section contains <1% skeletal grains,

comprising both bivalve fragments and echinoderms. Dismicrite/mudstone. The thin section sample contains just a couple very thin spar-filled fractures at various angles to bedding.

Unit 4: 0.85 m – moderate yellowish brown (10YR 5/4) calcareous mudstone. No bedding visible, occasional wispy laminations, and breaks into blocky pieces 2-3 mm wide dark grey shell fragments are present.

Unit 5: 0.83 m – greyish black (N2) dolomite with many spar-filled fractures sub-perpendicular to bedding; these range in size from <1 mm to .5 cm.

Thin section: Micrite matrix with ~5-30% skeletal grains. Grains show both original and recystrallized internal structure. Most are mollusc bivalves and echinoderms, with just a few gastropods. The skeletal grains are moderately to poorly sorted, with some bivalves subparallel to bedding but most other grains show no preferred orientation. Most molluscs are broken single valves. A moderate number of thin, sub-vertical spar-filled fractures are present. Sparse biomicrite/wackestone.

Unit 6: 0.50 m – medium yellowish brown (10YR 5/2) calcareous mudstone; no apparent bedding planes. 2-4 mm wide dark grey shell fragments present.

Unit 7: 0.27 m – dark grey (N3) dolomite, massive. No spar-filled fractures apparent in hand sample, but some un-filled fractures sub-perpendicular to bedding. Contains ***Shonisaurus* specimen UMNH VP 32545**, and associated in situ ammonoids *Tropites subquadratus* (UMNH IP 7017), *Tropites crassicostatus* (UMNH IP 7018, 7019, 7020, 7023, 7024, 7026), *Tropites* sp. (UMNH IP 7021, 7022), and cf. *Tropithisbites densicostatus* (UMNH IP 7025).

Thin section: Micrite matrix with 30-40% skeletal grains. Most grains retain internal structure, though some larger molluscs show partial recrystallization (with sparry matrix along some edges). Skeletal grain include mollusc bivalves, gastropods, rarer echinoderms, and one big ammonoid. Small (~1 mm) gastropods and bivalves are particular abundant. Larger bivalves are disarticulated with often broken edges, but a third to half of the small bivalves are articulated. Skeletal grains at the top of the thin section show some sub-parallel orientation (bivalve pieces), but the rest of the sample shows no preferred orientation. Some of the small molluscs are infilled with a much darker micrite mud than the main matrix. Peloids are fairly abundant infilling the large ammonoid, but occasionally present throughout the thin section. Spar-filled fractures are rare, and when present, are sub-vertical. There is one dark, interdigitating sub-vertical fracture that almost looks stylolitic. Sparse biomicrite/packstone.

Unit 8: 0.20 m – dark yellowish brown (10YR 4/2) calcareous mudstone. Some wispy laminations and small shell fragments. Deeply weathered with abundant modern roots.

Unit 9: 0.10 m – dark grey (N3) silty dolomite. No apparent bedding.

Thin section: Micrite matrix with pervasive patches of microspar, 10-25% skeletal grains. Skeletal grains dominated by mollusc bivalves and echinoderms, with rare gastropods. Most bivalves are disarticulated, but there are small (<1 mm) articulated bivalves. Larger but thin-shelled mollusc bivalves are prevalent with broken edges. Most skeletal grains show some degree of recrystallization, but some of the larger bivalves preserve original textures, whereas the small articulated bivalves are often completely recrystallized (including infilling matrix). Skeletal grains mostly display sub-parallel to

low angle orientation with bedding. Occasional peloids. Some thin, spar-filled fractures at ~30 degrees from vertical. Sparse biomicrite/wackestone.

Unit 10: 0.47 m – pale red (10R 6/2) calcareous mudstone slowly grading up into pale yellowish brown (10YR 6/2). Some wispy laminations and very small (<1 mm) dark grey shell fragments.

Unit 11: 0.20 m – dark grey (N3) dolomite with wispy mottles of dark yellowish orange (10YR 6/6). Some shells visible in hand sample cross-section on freshly-broken surfaces.

Thin section: Micrite matrix with many zones recrystallized into spar. 20-30% skeletal grains. Abundant mollusc bivalves of varying sizes, small gastropods (<2 mm), and echinoderms. Small bivalves and gastropods are typically recrystallized, but most echinoderms and larger bivalves display original structure, but often with adjacent recrystallized matrix. Larger bivalves are always disarticulated and often broken, but small bivalves (<1 mm) are articulated. The small bivalves and gastropods are often infilled by a very dark brown micrite mud that stands out in plain light. Most elongate skeletal grains are oriented sub-parallel with bedding. A few thin, vertical spar-filled cracks. Sparse biomicrite/packstone.

Unit 12: 1.40 m – dusky yellowish brown (10YR 2/2) calcareous mudstone with wispy laminations of dark yellowish orange (10YR 6/6). Some layers contain 1-2 mm shell fragments. ***Shonisaurus* specimen NVSMLV VM-2014-057-FS-002** is from approximately 1.1 m above the base of this unit.

Unit 13: 0.50 m – moderate olive brown (5Y 4/4) calcareous siltstone with no apparent bedding; breaks into block pieces. Basal 5 cm is more carbonate rich, is dark yellowish orange (10YR 6/6) and contains shells up to 6-7 mm wide (<1 mm thick). ***Shonisaurus***

specimens NVSMLV VM-2014-057-FS-001 and NVSMLV VM-2014-057-FS-003 are most likely from near the top of this unit, but could also have been found in Unit 14.

Unit 14: 0.20 m – dark grey (N3) dolomite with black shell fragments visible both on fresh broken surfaces and orange-colored weathered surfaces. Contains abundant ichthyosaur bone fragments, a chondrichthyan fin spine (UMNH VP 32541), and ammonoids including *Tropites* sp. (UMNH IP 7006, 7007), cf. *Discophyllites ebneri* (UMNH IP 7008), and *Arcestes* sp. (UMNH IP 7009).

Thin section: Micrite matrix with pervasive patches of microspar and a few zones of larger spar, 30-45% skeletal grains. Dominated by disarticulated & broken elongate, thin mollusc bivalves of varying sizes with subordinate small (<2 mm) articulated bivalves and rare echinoderms and small gastropods. A few disarticulated valves of ornamented bivalves as well. Possibly one brachiopod valve (hard to tell because of recrystallization). Grain size distribution trends towards being bimodal, though there is quite a bit of variation with the size of the larger thin mollusc bivalves. Most skeletal grains are partially or completely recrystallized. Elongate skeletal grains are largely sub-parallel to bedding, but there are zones where they show a more chaotic orientation. Some globular crystals of opaque/very dark red mineral, both isolated and in groups. Some very thin sub-vertical spar-filled fractures. Sparse biomicrite/packstone.

Unit 15: 0.85 m – moderate yellowish brown (10YR 5/4) slightly calcareous mudstone. No apparent bedding and breaks into tabular blocky pieces. Contains variably-sized (2 mm to 1 cm) black shell fragments.

Unit 16: 0.10 m – dark grey (N3) dolomite, massive, with occasional very thin (<1 mm) spar-filled fractures that are both sub-parallel and sub-perpendicular to bedding. No invertebrate fossils visible in hand sample.

Thin section: Micrite matrix with wispy dark zones and 1-5% skeletal grains. Isolated small zones of microspar. Skeletal grains dominated by very small (<1 mm) articulated mollusc bivalves, isolated echinoderm elements, and a few broken disarticulated thin bivalves. No apparent preferred orientation. Most skeletal grains except some echinoderms are recrystallized. Some very thin spar-filled fractures both sub-parallel to bedding and ~45° from bedding. Fossiliferous micrite/mudstone.

Unit 17: 0.50 m – pale yellowish brown (10YR 6/2) calcareous mudstone. Massive, and harder than most other mudstones in section.

Unit 18: 0.25 m – moderate yellowish brown (10YR 5/4) mudstone with carbonate in matrix. Occasional 1-2 mm shell fragments.

Unit 19: 0.10 m – medium dark grey (N4) dolomite; massive, with no visible bedding planes. Rare spar-filled fractures perpendicular to bedding. Abundant greyish black (N2) shells visible on freshly-broken surfaces and ammonoids. Collected ammonoid specimens UMNH VP 7012, 7013, 7014, and 7015 come from either this unit or Unit 21.

Thin section: Was originally micrite matrix, but now so heavily recrystallized in microspar that it can be difficult to distinguish even skeletal grains. 10-30% skeletal grains, almost all recrystallized, including variously-sized disarticulated and broken mollusc bivalves, small gastropods and articulated bivalves, and echinoderms. Some zones with skeletal grains sub-parallel to bedding whereas others show a high angle to bedding or no preferred orientation. Opaque/very dark red mineral pervasive throughout,

whether as very small crystals dispersed in matrix, blobs replacing parts of skeletal grains, larger cubic/rhombic crystals, and lining/filling sub-vertical fractures. Sparse biomicrite/wackestone.

Unit 20: 0.15 m – dark yellowish brown (10YR 4/2) calcareous mudstone. No apparent bedding planes. Thin (<1 mm) and wide (2-5 mm) shells are abundant.

Unit 21: 0.40 m – greyish black (N2) dolomite with some white (N9) spar-filled fractures that are 2 mm to 1 cm wide and sub-perpendicular to bedding. Weathered top surfaces of this unit display abundant shells. Collected ammonoid specimens UMNH VP 7012, 7013, 7014, and 7015 come from either this unit or Unit 19.

Thin section: Almost completely microspar matrix with just a few areas of micrite. 10-20% skeletal grains, dominated by elongate, thin, broken, disarticulated mollusc bivalves and rarer gastropods, though recrystallization makes identification difficult. A single large recrystallized ammonoid filled by large spar crystals. Skeletal grains are mostly sub-parallel to bedding, but a zone infilling the ammonoid displays sub-vertical bivalve pieces. Somewhat abundant small globular crystals of opaque/very dark red mineral. Abundant thin sub-vertical spar-filled fractures. Sparse biomicrite/wackestone.

Unit 22: 0.27 m – olive grey (5Y 3/2) calcareous mudstone with no apparent bedding planes. Contains 2-3 mm fragments of dark grey shell.

Unit 23: 0.12 m – brownish grey (5Y4 4/1) mudstone with weak laminations, not calcareous.

Unit 24: 0.58 m – very dusky red (10R 2/2) calcareous mudstone with no bedding and breaks into block pieces. Preserves large, complete black bivalve shells.

Unit 25: 0.10 m – dark grey (N3) dolomite. No observable bedding or spar-filled fractures.

Thin section: Similar to unit 19. Almost completely microspar matrix with just one zone of original micrite. Hard to distinguish skeletal grains in some areas because of recrystallization, but concentration appears to vary between 5-20%. Predominantly elongate thin-shelled broken disarticulated mollusc bivalves, but also echinoderms, gastropods, and small articulated bivalve. Some zones show some weak preferred orientation sub-parallel to bedding whereas others show no apparent preferred orientation. Abundant opaque/very dark red mineral throughout as small crystals dispersed in matrix and blobs replacing parts of skeletal grains, but particularly pervasive in uppermost layer where it also forms larger blobs and subhedral crystals. Sparse biomicrite/wackestone.

Unit 26: 0.50 m – pale red (10R 6/2) very calcareous mudstone. No apparent bedding and breaks into blocky pieces. Some horizons contain small (2-3 mm) shell fragments.

Quarry 6

At this outcrop, strata dip 40° to the east; strike of 56°.

Unit 1: 0.34 m – moderate olive brown (5Y 4/4) calcareous mudstone with occasional wispy laminations.

Unit 2: 0.10 m – dark grey (N3) dolomite with wisps of very pale orange (10YR 8/2) to pale yellowish orange (10YR 8/6) and ~1 to 8 mm wide bluish white (5B 9/1) spar-filled fractures sub-perpendicular to bedding. Unit breaks into flaggy pieces, but no observed bedding planes. Weather top-surfaces of bed display abundant black shell fragments.

Thin section: Micrite matrix, with a majority having been recrystallized into microspar, and 30-35% skeletal grains. Most skeletal grains are recrystallized, but some

retain original internal structure, and the small gastropods are filled by dark brown mud (no spar). Skeletal grains include mollusc bivalves, echinoderms, and gastropods, with bivalves being most abundant and largest in size. The skeletal grains are poorly sorted, but bivalves are typically parallel to sub-parallel to bedding, with a few zones where they are at higher angle because they have been "crunched" together prior to lithification. Occasional very small crystals of an opaque/very dark red mineral. A number of nearly vertical spar-filled fractures. Sparse biomicrite (though not too far from packed biomicrite)/packstone.

Unit 3: 1.49 m – olive grey (5Y 3/2) calcareous mudstone with very weak occasional laminations. Black shell fragments (1-3 mm) present in some horizons. This is the most likely unit to have produced the ***Shonisaurus*** **specimens NVSMLV VM-2014-057-FS-009-001 and UMNH VP 32538**.

Unit 4: 0.25 m – greyish black (N2) dolomite with bluish white (5B 9/1) spar-filled fractures at various angles. No bedding planes visible. Ichthyosaur bone fragments present.

Thin section: Micrite matrix with dark wispy laminations, isolated small microspar crystals, and 10-20% skeletal grains (varies throughout section). The skeletal grains are moderately to poorly sorted, and at a moderate to high angle to bedding; all are recrystallized. Skeletal grains are dominated by bivalves, with some gastropods and possibly a few echinoderms (hard to tell because of recrystallization). About half of the bivalves are small articulated specimens, and the other half are disarticulated larger valves. Moderate to pervasive very thin spar-filled fractures at a high angle to bedding, with occasional large spar-filled fractures parallel to bedding. Sparse biomicrite/wackestone.

Unit 5: 0.38 m – dark grey (N3) dolomite with some horizontal bedding and breaks into flat 1-2 cm thick pieces.

Thin section: Middle third of thin section is almost identical to Unit 4, except that the skeletal grains are parallel/sub-parallel to bedding, fining upwards, with an abrupt lower boundary. The rest of the thin section is micrite matrix with abundant but isolated small microspar crystals, and 3-5% recrystallized skeletal grains. These skeletal grains are almost exclusively bivalves, mostly parallel to bedding, and often broken. This part of the thin section is a fossiliferous micrite/mudstone. Occasional spar-filled fractures at high angle to bedding cross-cut the entire thin section.

Unit 6: 0.54 m – olive grey (5Y 4/2) slightly calcareous mudstone. No visible laminations or bedding planes, but breaks into blocky tabular pieces.

Unit 7: 0.01 m – olive grey (5Y 3/2) calcareous mudstone with large (~5 mm thick) spar-filled fracture that is very light grey (N8). Harder than underlying and overlying unit.

Unit 8: 1.25 m – moderate olive grey (5Y 4/2) very calcareous mudstone. No visible bedding, but breaks into blocky/tabular pieces.

Unit 9: 0.05 m – medium dark grey (N4) dolomite with very light grey (N8) spar-filled fractures up to 7 mm wide. No apparent bedding or fossils visible in hand sample.

Thin section: Micrite matrix with 50% small microspar crystals (?dolomite) and less than 1% skeletal grains (except at very top of thin section, where skeletal grains are a bit more abundant). All skeletal grains are heavily recrystallized, making identification difficult; those that can be ID'd are small articulated mollusc bivalves at various angles to

bedding. Moderate number of spar-filled fractures at high angle to bedding. Dismicrite/mudstone.

Unit 10: 0.80 m – moderate yellowish brown (10YR 5/4) very calcareous mudstone. No apparent bedding but breaks into blocky/tabular pieces. Small (2-3 mm) dark grey shell fragments sometimes present.

Unit 11: 0.15 m – dark grey (N3) dolomite with blotches of pale yellowish orange (10YR 8/6), and extensive bluish white (5B 9/1) spar-filled fractures that are often sub-perpendicular to bedding.

Thin section: Nearly completely recrystallized into microspar, with less than 10% micrite. Skeletal grains appear as recrystallized "ghosts"; abundance estimate and identification is thus very difficult, but probably between 5-20% skeletal grains that include bivalves and other unidentified fossils. Stylolites are present in a couple of zones. Very pervasive spar-filled fractures at both low and high angle to bedding. If the original matrix was micrite, then would have been a sparse biomicrite/wackestone.

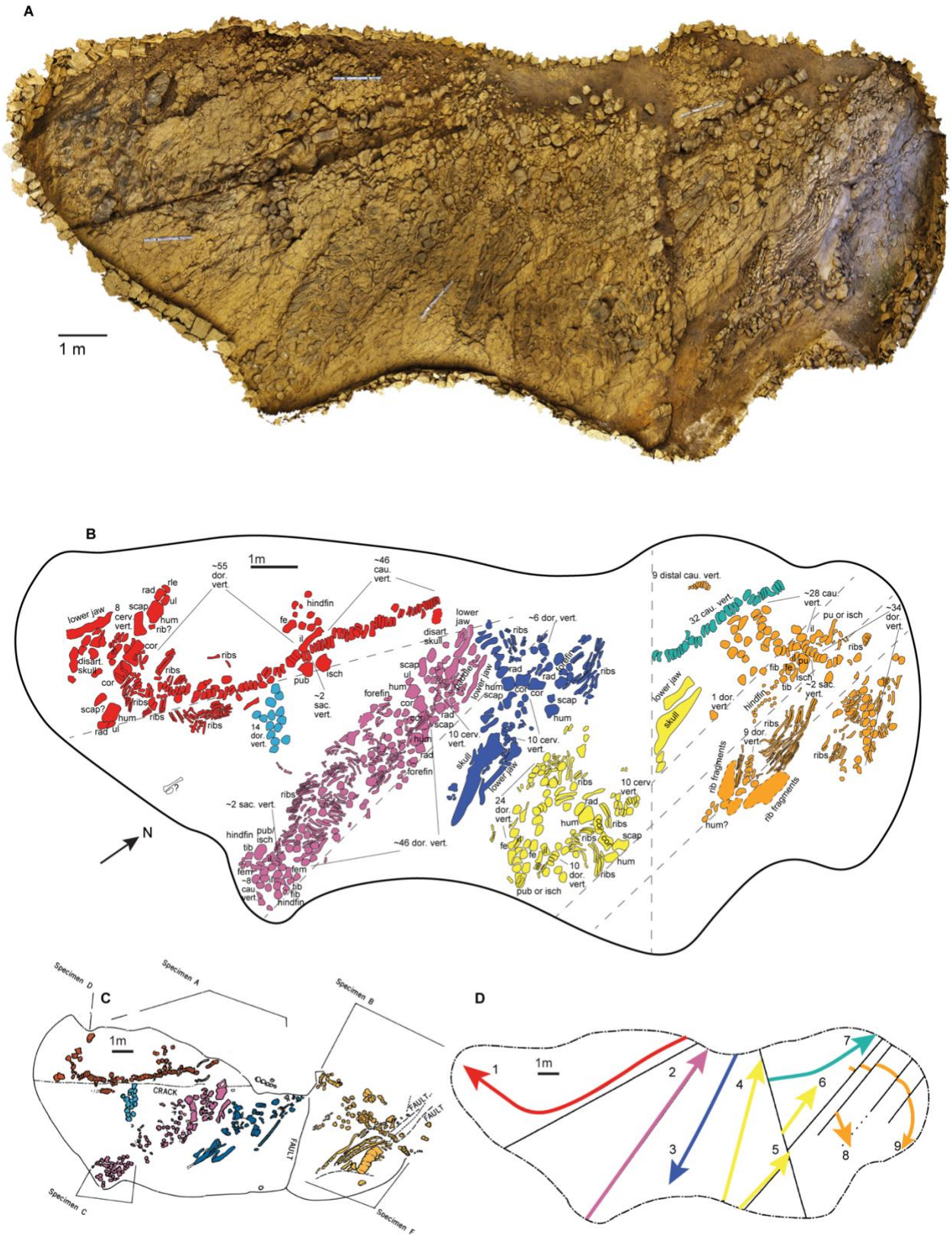
A
1 m
B
1m
N
lower jaw
8 cerv vert.
rad
rle
scap
ul
hum
rib?
cor
disart. skull
ribs
scap?
rad
ul
~55 dor. vert.
hindfin
fe
il
pub
isch
~2 sac. vert.
14 dor. vert.
~46 cau. vert.
lower jaw
disart. skull
~6 dor. vert.
ribs
rad
radius
cor
scap
hum
forefin
ul
10 cerv. vert.
skull
lower jaw
24 dor. vert.
10 cerv vert.
10 dor. vert.
pub or isch
~46 dor. vert.
~2 sac. vert.
hindfin
pub/ isch
tib
fem
~6 cau. vert.
fib
9 distal cau. vert.
32 cau. vert.
~28 cau. vert.
pu or isch
~34 dor. vert.
1 dor. vert.
~2 sac. vert.
9 dor. vert.
rib fragments
hum?
C
Specimen D
Specimen A
Specimen B
Specimen C
Specimen F
1m
CRACK
FAULT
FAULT
FAULT
D
1m
1
2
3
4
5
6
7
8
9

Figure S1. Interpretation of Quarry 2, related to Figure 2 and S2. (A) Raw orthographic composite photo of Quarry 2; **(B)** Detailed map of Quarry 2 based on 3D scanning data and detailed observations of the site. Colors follow Figures 2 and 3. Dashed lines depict faults. Abbreviations: cau. vert. – caudal vertebrae; cerv. vert. – cervical vertebrae; cor – coracoid; dor. vert – dorsal vertebrae; fe – femur; fib – fibula; hum – humerus; il – ilium; isch – ischium; pub – pubis; rad – radius; rle – radiale; sac. vert. – sacral vertebrae; scap – scapula; tib – tibia; ul – ulna; **(C)** Quarry map made during the original excavations adapted from ref. S1. Note that not all skeletons had been fully excavated when this map was made; **(D)** Diagrammatic quarry map adapted from ref. S2.

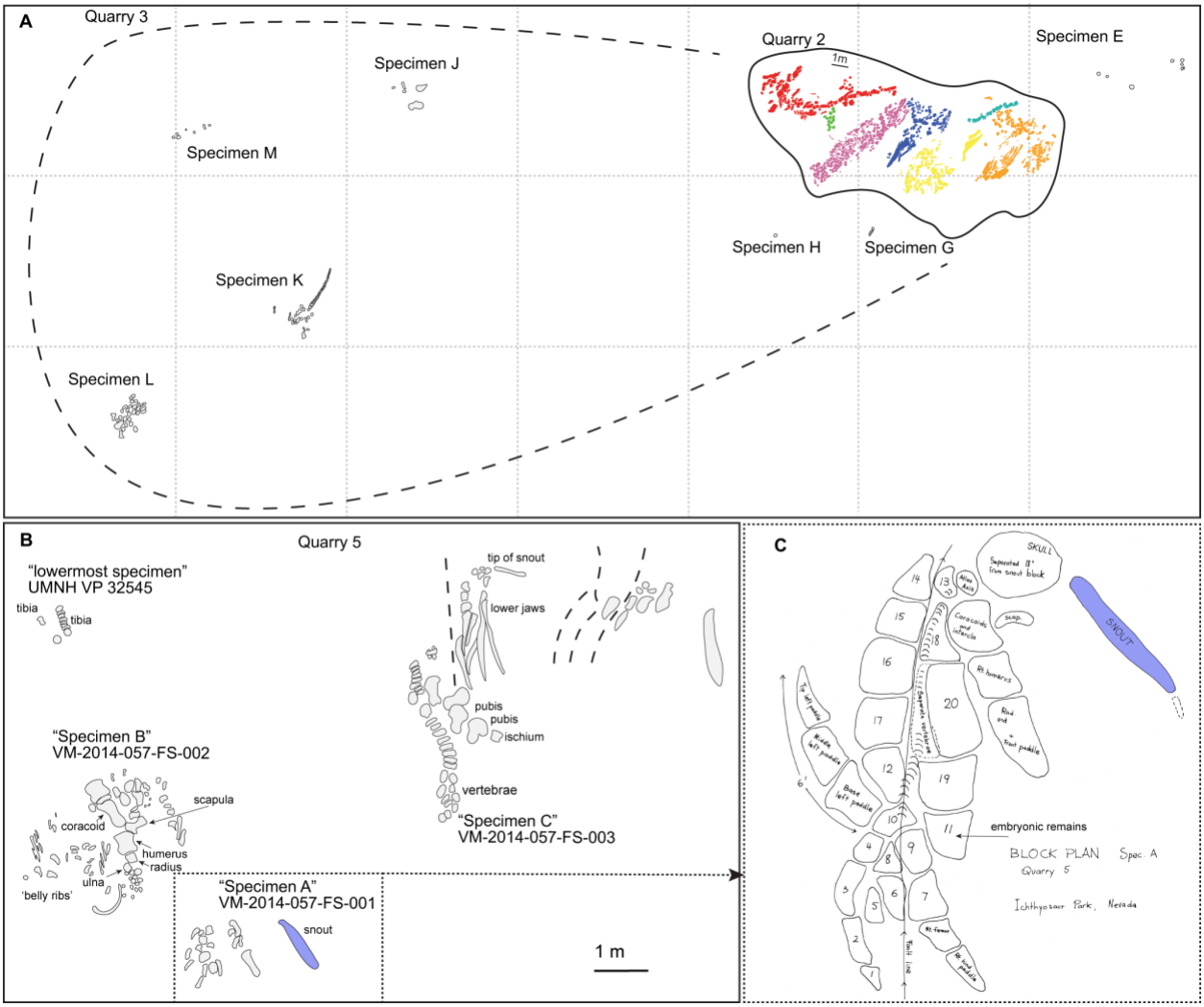

Figure S2. Additional WUC Quarries, related to Figures 1, 2 and S1. (A) Map of Quarry 3 specimens scattered across a broad area in the vicinity of Quarry 2, grid is 10 m by 10 m; **(B)** Map of Quarry 5, including type series ('Specimens A-C') note and one additional specimen UMNH VP 32545 partially excavated during recent field seasons. Note that not all specimens had been fully excavated with this map was made; **(C)** Block diagram of type specimen, VM-2014-057-FS-00, created during excavation, arrow indicates where embryonic remains were observed in block 11. Blue shading is same element in panels b. and c. to assist the reader in registering these two maps with each other. All maps adapted from unpublished documents housed in the archives of the University of California Museum of Paleontology.

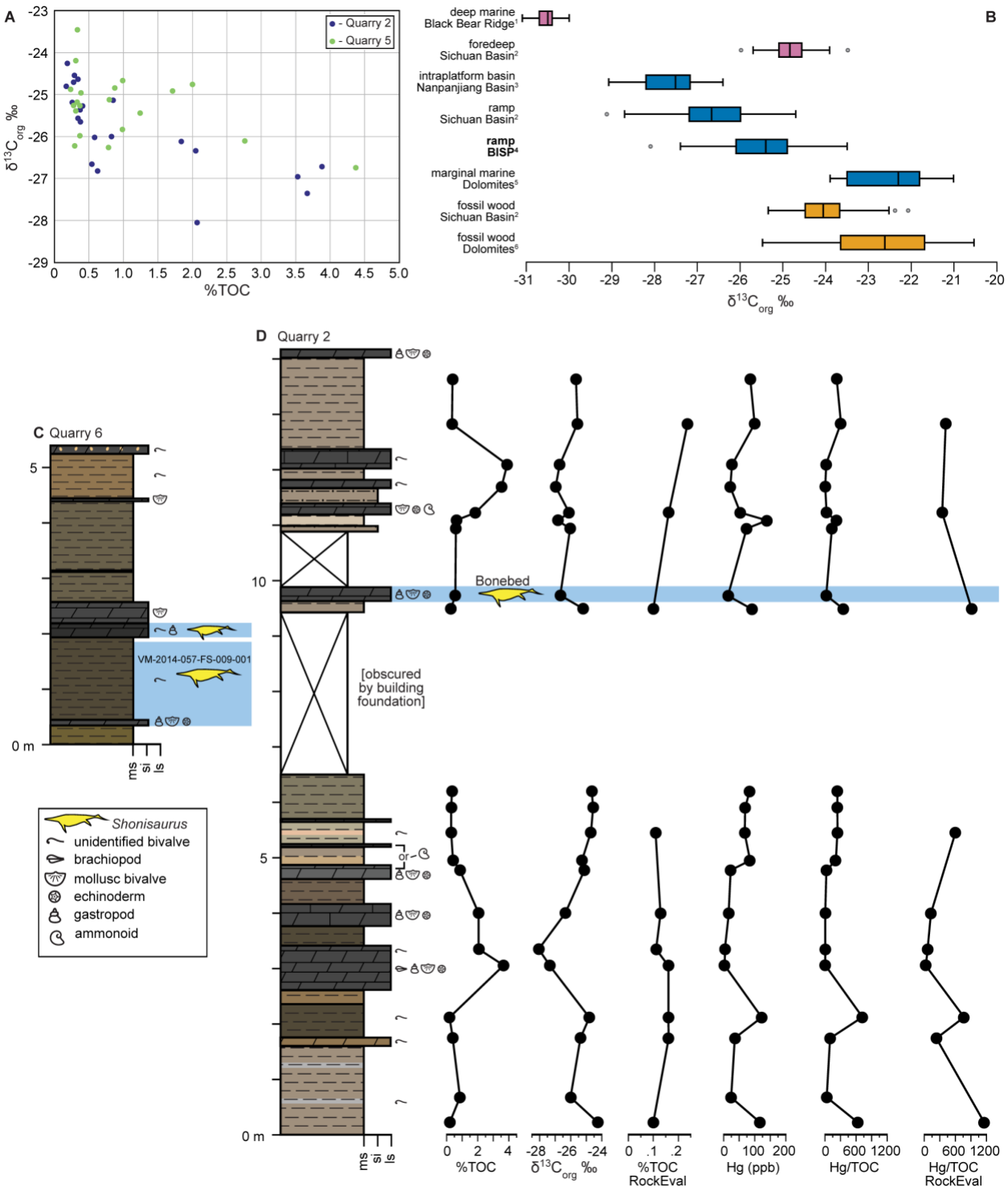
A
- Quarry 2
- Quarry 5
δ13Corg ‰
%TOC
B
deep marine
Black Bear Ridge1
foredeep
Sichuan Basin2
intraplatform basin
Nanpanjiang Basin3
ramp
Sichuan Basin2
ramp
BISP4
marginal marine
Dolomites5
fossil wood
Sichuan Basin2
fossil wood
Dolomites6
δ13Corg ‰
C Quarry 6
VM-2014-057-FS-009-001
0 m
ms
si
ls
D Quarry 2
Bonebed
[obscured
by building
foundation]
or
0 m
Shonisaurus
unidentified bivalve
brachiopod
mollusc bivalve
echinoderm
gastropod
ammonoid
%TOC
δ13Corg ‰
%TOC
RockEval
Hg (ppb)
Hg/TOC
Hg/TOC
RockEval

Figure S3. Additional geochemical data from WUC, related to Figure 1. **(A)** Cross-plot of total organic carbon content (TOC) and organic $\delta^{13}C$ isotopic values for bulk samples from Quarry 2 and Quarry 5 (see main text Figure 1); **(B)** Box plots of the range of $\delta^{13}C_{org}$ values from different depositional environments in Carnian strata, re-drafted and modified from Jin et al.[S3] Grey dots are individual outlier values. Data sources are 1: Williford et al.[S4], 2: Jin et al.[S3], 3: Sun et al.[S5], 4: this paper, 5: Dal Corso et al.[S6], and 6: Dal Corso et al.[S7]; **(C)** Measured stratigraphic section for Quarry 6; **(D)** Mercury (Hg) concentration data for Quarry 2 (see main text figures 1–2). Note that the different TOC values for '%TOC' and '%TOC RockEval' are because the latter were measured prior to acid digestion of the sample, whereas the former were measured after digestion. Importantly, both sets of measurements show the same trends when used to normalize Hg concentrations.

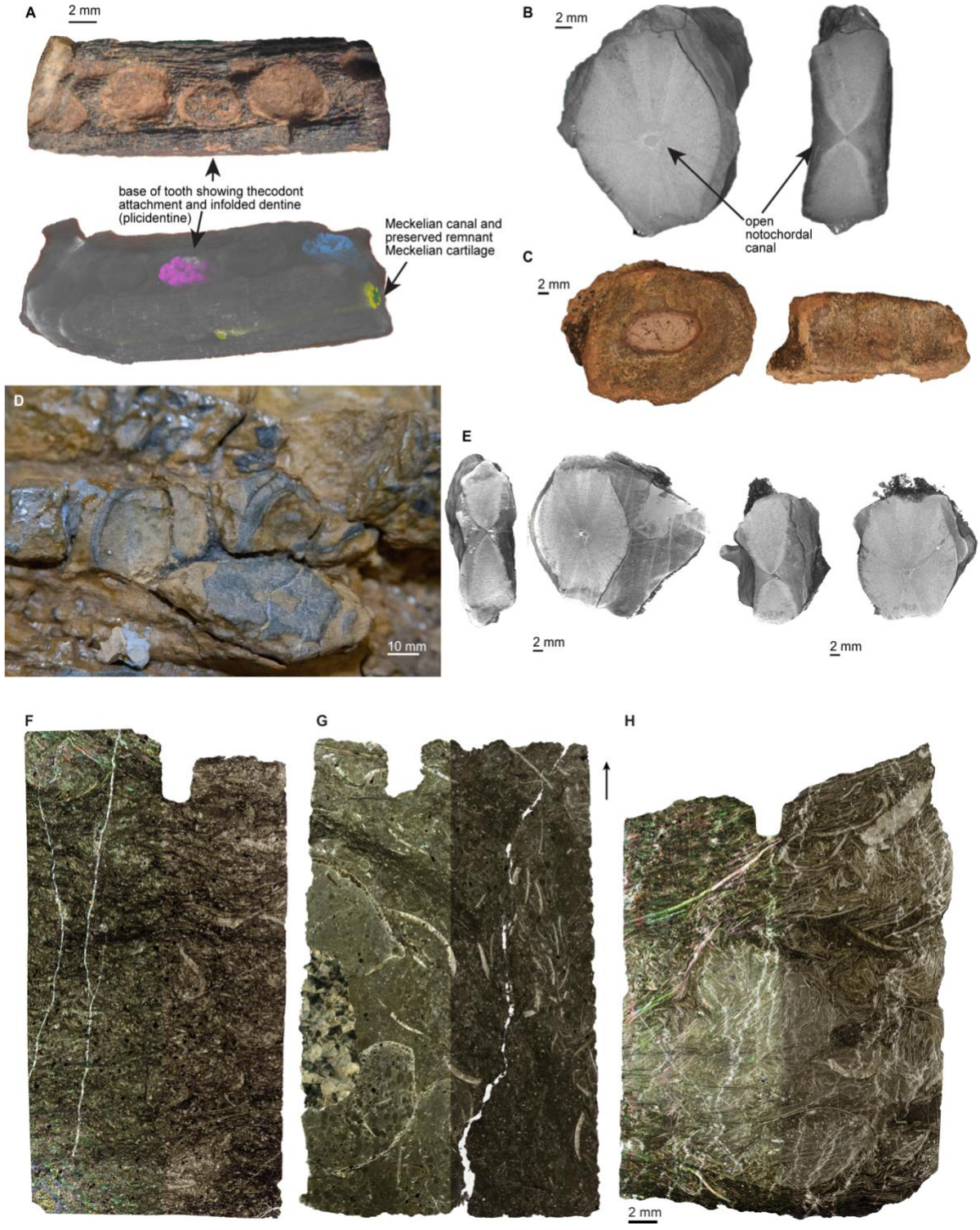
A
2 mm
base of tooth showing thecodont attachment and infolded dentine (plicidentine)
Meckelian canal and preserved remnant Meckelian cartilage
B
2 mm
open notochordal canal
C
2 mm
D
10 mm
E
2 mm
2 mm
F
G
H
2 mm

Figure S4. Photographs and µCT scans of additional *Shonisaurus* embryo specimens and petrographic thin sections, related to Figures 1 and 3. (A) Partial jaw UCMP 290269 identified in collections; **(B)** Isolated vertebra VM-2014-057-FS-007 identified in collections; **(C)** isolated vertebra UMNH VP 32547 collected in the field; **(D)** Closeup of *in situ* embryonic centra from *Shonisaurus* type specimen, VM-2014-057-FS-001, "Specimen A" of Camp, removed for CT scanning (compare Figure 3h); **(E)** µCT scans of centra shown in panel D; **(F)** Main bonebed horizon in Quarry 2; **(G)** UMNH VP 32545 horizon in Quarry 5 (see main text Figure 1); **(H)** NVSMLV VM-2014-057-FS-001 (*Shonisaurus popularis* holotype) and VM-2014-057-FS-003 horizon in Quarry 5 (see main text Figure 1). Left side of each thin section is in cross-polarized light, right side is in plain polarized light. Arrow indicates stratigraphic up.

Locality	Specimen	Centrum width	Centrum Length	Humerus Length	Coracoid Length
Quarry 2 (Display Quarry)	Specimen I	28.8	7.1	44.5	50.85
	Specimen II	28.8	7.2		
	Specimen III	21	6.5	31.5	36.4
	Specimen IV	21.3	7	31.1	31.8
	Specimen Vb	21.4	6.8	37.8	35.7
	Specimen VIc	23.4	9.6		
	Specimen VII	24.4	8.2		
Quarry 5 (Type Locality)	Specimen A*	22	7.5	40	47
	Specimen B*	18	6	37	39
	UMNH VP 32545	20	6		
	VM-2014-057-FS-010-001**	3	1		
	VM-2014-057-FS-001**	3.5	1.25		
Other Locality	Vertebra from Quarry 6*	27.5	9		
	UMNH VP 32539			41	50
	UMNH VP 32547**	2.25	1		
	VM-2014-057-FS-006-001*			36	
	UMNH VP 32546	21	6.5		
	UMNH VP 32544	21	6.8		

* Measurement taken from ref *6*.
** Denotes embryo/neonate

Table S1. Measurements of selected specimens, related to Figure 3. All units are cm.

Locality	Sample	Stratigraphic Position (m)	TOC (Wt%)	$\delta^{13}C_{org}$ (‰) (VPDB)	$TOC_{RockEval}$ (Wt%)	Hg (ppb)	Hg/TOC	$Hg/TOC_{RockEval}$
Quarry 2	BISP-02-01	0.15	0.2	-24.3	0.1	116	629.1	1160.0
	BISP-02-02	0.6	0.8	-26.0		24	29.0	
	BISP-03-01	1.68	0.4	-25.4	0.16	37	99.2	231.3
	BISP-04-01	2.05	0.2	-24.8	0.16	122	720.9	762.5
	BISP-06-01	3	3.7	-27.4	0.16	2.6	0.7	16.3
	BISP-06-02	3.3	2.1	-28.1	0.11	6.4	3.1	58.2
	BISP-08-01	3.95	2.1	-26.3	0.13	16	7.8	123.1
	BISP-10-01	4.73	0.9	-25.1		22	25.9	
	BISP-11-01	4.9	0.4	-25.3		84	207.2	
	BISP-13-01	5.42	0.3	-24.7	0.11	67	240.8	609.1
	BISP-15-01	5.87	0.3	-24.5		69	239.3	
	BISP-15-02	6.17	0.3	-24.6		83.5	246.7	
	BISP-17-01	9.45	0.3	-25.2	0.1	92	361.0	920.0
	BISP-18-01	9.7	0.5	-26.7		15.5	28.5	
	BISP-20-01	10.9	0.6	-26.0		74.5	128.0	
	BISP-21-01	11.05	0.6	-26.8		139.5	222.8	
	BISP-22-01	11.2	1.8	-26.1	0.16	54	29.4	337.5
	BISP-24-01	11.67	3.5	-27.0		22.5	6.4	
	BISP-26-01	12.07	3.9	-26.7		26.5	6.8	
	BISP-27-01	12.82	0.3	-25.6	0.24	101	297.0	420.8
	BISP-27-02	13.62	0.4	-25.7		86.5	231.2	
Quarry 5	BISP-16-11	0.57	2.0	-24.8				
	BISP-16-12	1.07	0.3	-24.2				
	BISP-16-14	1.62	0.3	-23.5				
	BISP-16-15	2.52	1.7	-24.9				
	BISP-16-16	3.25	0.3	-25.2				
	BISP-16-17	3.55	2.8	-26.1				
	BISP-16-19	4.17	0.3	-26.2				
	BISP-16-20	4.69	0.9	-24.8				
	BISP-16-21	5.74	0.3	-25.3				
	BISP-16-22	6.34	0.2	-24.9				
	BISP-16-23	6.74	0.4	-26.0				
	BISP-16-24	7.24	1.2	-25.4				
	BISP-16-25	7.74	1.0	-24.7				
	BISP-16-26	8.19	0.4	-25.3				
	BISP-16-27	8.39	0.3	-25.4				
	BISP-16-28	8.59	0.4	-25.0				
	BISP-16-29	8.99	4.4	-26.7				
	BISP-16-30	9.29	0.8	-25.1				
	BISP-16-31	9.87	1.0	-25.8				
	BISP-16-32	10.21	0.8	-26.3				

Table S2. Quarries 2 and 5 bulk total organic carbon (TOC), organic carbon stable isotope ($\delta^{13}C_{org}$), and, for Quarry 2 only, mercury (Hg) concentration data, related to Figure 1 and Figure S3.

	SkU	Camp Spec. ID	Ref. *S2* ID#	Ref. *S1* Spec.#	Description & comments	Status & Current Specimen #s
Quarry 1	*	-	-		Crushed but largely complete skull and associated limb elements, excavated by Camp in 1953. Formerly on display in Visitor's quarry. Current status unknown.	Unknown
Quarry 2 (Fossil Shelter)	I*	Specs. A (part) & D	1		Largest and most complete specimen in Visitor's quarry including posterior skull, girdles and proximal limbs, most of axial skeleton except distal tail, ribs. Orientation originally misinterpreted by Camp. Anterior skull may continue below quarry wall.	On display at BISP
	II*	"front paddle"	-		Cluster of large, fully disarticulated but tightly packed vertebrae, apparently not derived from nearby SU I. Originally misinterpreted by Camp as front paddle bones.	On display at BISP
	III*	Spec. C	2		Smallest individual on display based on femoral length & vertebral diameter. Largely complete and associated but disarticulated. Anterior skull terminates at quarry boundary and distalmost portion missing. Tail may extend below quarry wall. Jaw preserves at least four alveoli.	On display at BISP
	IV*	Spec. A (part)	3		Anterior half of skeleton. Moderately disarticulated. Terminates mid-torso at quarry boundary and posterior half is missing. Originally interpreted by Camp as connected to SU I.	On display at BISP
	Va*	-	4		Posterior torso and pelvic girdle, moderately disarticulated but associated. Absent from Camp's published quarry map (Camp 1980, Figure 2) but seems to be in situ and revealed by later excavation.	On display at BISP
	Vb*	-	5		Anterior torso (including cervical vertebrae) and pectoral girdle, moderately disarticulated but associated. Absent from Camp's published quarry map (Camp 1980, Figure 2) but seems to be in situ and revealed by later excavation	On display at BISP
	Vc*	-	7		Anterior skull, crushed. Absent from Camp's published quarry map (Camp 1980, Figure 2). excavated later by Sam Welles? On display at Visitor's quarry. Aligned with Vb but cut by fault, posterior skull missing. Faulted upward & weathered away before discovery?	On display at BISP
	Via*	Spec. F	8		Semi-articulated dorsal vertebrae and ribs, as well as a portion of a proximal forelimb sheared by a fault. This specimen was considered by Camp to be "18 inches" (~46 cm) higher than the main quarry level. This specimen has been extensively shorn up with cement along a highly faulted and fractured portion of the quarry.	On display at BISP
	VIb*	Spec. B	9		Disarticulated dorsal vertebrae and ribs on a lower, down faulted level. Several vertebrae are aligned in a two tightly packed parallel rows. Some vertebrae are bisected by faults. This lower portion of the quarry floods on occasion and some vertebrae are partially buried in mud.	On display at BISP
	Vic*	Spec. B	9		Semi-articulated posterior dorsal and sacral and disarticulated anterior caudal vertebrae along with associated pelvic girdle elements and an associated right hindlimb—the most complete paddle in the quarry.	On display at BISP
	Vid*	-	9		A short string of nine articulated distal caudal vertebrae. Camp's original quarry diagram indicates that this string may have been moved and rotated, and other short strings of semi-articulated and disarticulated distal caudal vertebrae figured by Camp in this area of the quarry are now seemingly missing.	On displayat BISP
	VII*	-	6		String of approximately 32 articulated and semi-articulated caudal vertebrae. This specimen does not appear on Camp's original quarry diagram but seems to be in situ and revealed by later excavation.	On display at BISP
	-	Spec. E	-		*"A few vertebrae at extreme northeast of quarry"* – Camp field notes August 29, 1954. Current status unknown, based on field map outside of limits of present fossil shelter display.	Unknown
Quarry 3	-	Spec. G	-		*"Vertebrae and ribs 4' above level [of Quarry 2]"* – Camp field notes August 29, 1954. Current status unknown, based on field map outside of limits of present fossil	Unknown

					shelter display. Closer to Quarry 2 than other 'Quarry 3' specimens, but evidently from a distinct horizon unless faulted.	
	*	Spec. H	-		*"Vertebra (13.5") and limb bones 16 feet(?) up"*– Camp field notes August 29, 1954. Scattered bone was found by Camp in abundance on a higher stratigraphic level upslope from Quarry 2, but in situ specimens were lacking despite extensive prospecting. Recent field work by the authors confirms scattered bone fragments in this vicinity.	Unknown
	*	Spec. J	-		Skull and limb fragments partially excavated by Camp in 1954 & 1955 based on field notes and maps. Approximately 20 meters southwest of fossil shelter corresponding to parking lot today.	Unknown reburied?
	*	Spec. K	-		Semi articulated tail, associated pelvic girdle and hind limb elements. Approximately 20 meters south of specimen J and about 33 meters southwest of fossil shelter. Also referred to as 'big hip' and 'big hips' in Camp field notes. A portion of this specimen is still visible in exposed tail adjacent to parking lot of fossil shelter. More of the specimen may be buried. One femur stolen per Camp field notes May 27, 1957.	Exposed outside of fossil shelter at BISP
	*	Spec. L	-		"*a large femur, tibia, vertebrae and hind paddle bones, fragments of ribs*" – Camp field notes October 23, 1954. Current status unknown. Also referred to as 'Stewart's tail' and 'Stewart-Keeler tail' in Camp field notes (or this reflects confusion with Specimen K?). Camp describes the location as '50 feet (~15 m) south' of Specimen. K.	Unknown reburied?
	-	Spec. M	-		Little information available about this specimen, Camp mentions working on it but cannot find a specific description in field notes. In one place Camp also indicates "big hips" as an alternate name but that is more typically associated with Specimen K in his notes. Field map indicates ~7 scattered vertebrae, about 20 m southwest of Specimen J?	Unknown
	-	Spec. N	-		Fragmentary specimen only mentioned in passing in Camp notes. "*60 feet south of the big hips* [Specimen K or M]"	Unknown
Quarry 4	*	'*S. mulleri*' holotype	-	FZVE-5	"*well preserved pelvis, femur, part of a hind paddle and a rib*" – Camp 1980. Camp regarded this locality as ~120 meters lower in stratigraphic section than Quarries 2 (fossil shelter) and 5 (type locality) in the lower macrolobatus ammonoid zone. An associated forelimb was also reported from this vicinity and the authors located additional scattered bones in this area. Now in Nevada State Museum, Las Vegas collections.	NVSM-LV collections VM-2014-057-FS-008
Quarry 5 (Type Locality)	*	A-5	-	FZVE-1	Most complete specimen and holotype of *Shonisaurus popularis*. Skull, limbs, girdles, vertebrae, ribs & gastralia all largely preserved. Extensively described and figured by Camp 1980. Contains in situ embryo. Now in Nevada State Museum, Las Vegas collections.	NVSM-LV collections VM-2014-057-FS-001
	*	B-5	-	FZVE-2	*"Specimen B-5 lay about 3 m north of and about 0.90 m below the much more complete Specimen A-5…. scapula, coracoid, humerus, radius and ulna, carpals, and proximal phalanges together with a series of anterior ribs, separate rib ends, cervical vertebrae and skull fragments."* – Camp 1980 Paratype of *Shonisaurus popularis.* Extensively described and figured by Camp 1980.	NVSM-LV collections VM-2014-057-FS-002
	*	C-5	-	FZVE-3	"*A more complete series of caudal vertebrae, 68 in all, … This one lay parallel to Specimen A, apparently on the same level and only a few feet to the east of A. Specimen C, a smaller individual, consisted of the tail, the pelvis, femora, tibiae, a fibula, a few paddle bones, fragments of ribs and weathered dorsal vertebrae and a skull eight feet in length. In this skull the elements of the lower jaw had been macerated apart and lay separated in the matrix. The rear elements were badly eroded. The rostrum was complete and still bore one complete remaining tooth.*" – Camp 1980. Paratype of *Shonisaurus popularis.* Extensively described and figured by Camp 1980.	NVSM-LV collections VM-2014-057-FS-003

	-	"lowermost"	-		*"A single skeletal section with dorsal vertebrae, ribs, femur and a tibia*" Camp 1980. ~1.8 meters below Specimen B-5 per Camp 1980. Left uncollected by Camp. Dorsal vertebrae disarticulated in fashion similar to some Quarry 2 (fossil shelter) specimens. Further excavated in 2016–2019 by UNMH.	Partially collected UMNH VP 32545
	-	Unnamed Q5	-		"*Less than 30 cm above ["lowermost" specimen]…a series of 38 anterior caudal vertebrae lying parallel to the skeleton below and evidently not a part of that skeleton*."	Unknown
	-	Additional fragmentary specimens	-		"*Scattered parts of at least four individuals lie from 8 to 30 m east and northeast of Specimen C, and two large, isolated centra lay a foot or so immediately above its tail."* – Camp 1980. Abundant scattered bone was observed by the authors in this quarry, some of it in situ, most weathered out on the surface.	Unknown
Quarry 6	-	Unnamed Q6 specimen	-		"*About 300 m to the east of C, near the hilltop at Quarry 6, parts of a larger skeleton appeared in a steeply dipping layer of hard limey shale. We failed to excavate this skeleton owing to the steep dip of the beds.*" –Camp 1980. Large vertebrae, limb and girdle elements and skull fragments reported by Camp in field notes (at least the vertebrae were collected & now in Las Vegas collections). Camp tried to excavate but proved too difficult. Authors relocated this quarry and found abundant scattered bone as well as some in situ. One large humerus from this quarry was collected by NHMU but unclear if it represents the same or a different specimen.	NVSM-LV collections VM-2014-057-FS-009 Humerus: UMNH VP 32538
Quarries 7–9	-	Unnamed Q7-9 specimens	-		*"To the south and southwest of Quarry 6, for a distance of nearly 800 m, isolated and eroded parts of skeletons lie on the surface and extend to shallow depths along steeply dipping beds. None of these was collected."*—Camp 1980. The authors relocated this general area and confirmed the presence of abundant bone weathering out on the surface at multiple horizons.	Uncollected
Quarry X	*	*'S. silberlingi'* holotype	-	FZVE-7	Left humerus, left radius, ulnare, and large neural spine. Regarded by Camp as stratigraphically ~150 meters below Quarries 2 & 5 and 30 meters below Quarry 4 in the schucherti ammonoid zone. Now in Nevada State Museum, Las Vegas collections.	NVSM-LV collections VM-2014-057-FS-006-001
NHMU Quarry	*	-	-		New specimen discovered in 2014 by UNMH—Smithsonian—UNR team. Specimen includes partial skull, dorsal vertebrae, ribs, partial forelimb, pectoral girdle, hindlimb, and pelvic girdle elements. In NHMU collections under study by the authors.	Collected by UNMH UMNH VP 32539

* Denotes specimen included in taphonomic analysis.

Table S3. Indivdual descriptions of WUC *Shonisaurus* specimens, related to Figures 2, S1 and S2 and Table 1. Quotes from ref. S1 and unpublished field notes kept in the archives of the University of California Museum of Paleontology.

Supplementary References

S1. Camp, C.L. (1980). Large ichthyosaurs from the Upper Triassic of Nevada. Palaeontographica Abt. A *170*, 139–200.

S2. Hogler, J.A. (1992). Taphonomy and paleoecology of *Shonisaurus popularis* (Reptilia: Ichthyosauria). Palaios *7*, 108–117. 10.2307/3514800

S3. Jin, X., McRoberts, C.A., Shi, Z., Mietto, P., Rigo, M., Roghi, G., Manfrin, S., Franceschi, M. and Preto, N. (2019). The aftermath of the CPE and the Carnian-Norian transition in northwestern Sichuan Basin, South China. J. Geol. Soc. *176*, 179–196. 10.1144/jgs2018-104

S4. Williford, K. H., Orchard, M. J., Zonneveld, J.-P., McRoberts, C. and Beatty, T.W. (2007). A record of stable organic carbon isotopes from the Carnian-Norian boundary section at Black Bear Ridge, Williston Lake, British Columbia, Canada. Albertiana *36*, 146–148.

S5. Sun, Y.D., Wignall, P.B., Joachimski, M.M., Bond, D.P., Grasby, S.E., Lai, X.L., Wang, L.N., Zhang, Z.T. and Sun, S. (2016). Climate warming, euxinia and carbon isotope perturbations during the Carnian (Triassic) crisis in South China. Earth and Planet. Sci. Lett. *444*, 88–100. 10.1016/j.epsl.2016.03.037

S6. Dal Corso, J., Gianolla, P., Rigo, M., Franceschi, M., Roghi, G., Mietto, P., Manfrin, S., Raucsik, B., Budai, T., Jenkyns, H.C. *et al*. (2018). Multiple negative carbon-isotope excursions during the Carnian Pluvial Episode (Late Triassic). Earth Sci. Rev. *185*, 732–750. 10.1016/j.earscirev.2018.07.004

S7. Dal Corso, J., Mietto, P., Newton, R. J., Pancost, R. D., Preto, N., Roghi, G., and Wignall, P. B. (2012). Discovery of a major negative $\delta^{13}C$ spike in the Carnian (Late Triassic) linked to the eruption of Wrangellia flood basalts. Geology *40*, 79–82. 10.1130/G32473.1

S8. McGowan, C. and Motani, R. (1999). A reinterpretation of the Upper Triassic ichthyosaur *Shonisaurus*. J. Vert. Paleontol. *19*, 42–49. 10.1080/02724634.1999.10011121

S9. Houssaye, A., Nakajima, Y., & Sander, P. M. (2018). Structural, functional, and physiological signals in ichthyosaur vertebral centrum microanatomy and histology. Geodiversitas *40* 161–170.

S10. Nicholls, E.L. and Manabe, M. (2004). Giant ichthyosaurs of the Triassic—a new species of *Shonisaurus* from the Pardonet Formation (Norian: Late Triassic) of British Columbia. J.

S11. Ji, C., Jiang, D. Y., Motani, R., Rieppel, O., Hao, W. C., and Sun, Z. Y. (2016). Phylogeny of the Ichthyopterygia incorporating recent discoveries from South China. J. Vert. Paleontol. *36* e1025956. 10.1080/02724634.2015.1025956

S12. Moon, B. C. (2019). A new phylogeny of ichthyosaurs (Reptilia: Diapsida). J. Syst. Palaeontol. *17*, 129–155. 10.1080/14772019.2017.1394922

S13. Sander, P.M., Chen, X., Cheng, L. and Wang, X. (2011). Short-snouted toothless ichthyosaur from China suggests Late Triassic diversification of suction feeding ichthyosaurs. PLoS ONE 6, e19480. 10.1371/journal.pone.0019480

S14. Callaway, J.M. and Massare, J.A. (1989). *Shastasaurus altispinus* (Ichthyosauria, Shastasauridae) from the Upper Triassic of the El Antimonio district, northwestern Sonora, Mexico. J. Paleontol. *63*, 930–939.

S15. McGowan, C. and Motani, R. Handbook of Paleoherpetology: Vol. 8 Ichthyopterygia. (2003) (Verl. Dr. Friedrich Pfeil, Munich).

S16. Adams, T.L. (2009). Deposition and taphonomy of the Hound Island Late Triassic vertebrate fauna: fossil preservation within subaqueous gravity flows. Palaios *24*, 603–615. 10.2110/palo.2009.p09-010r

S17. Dalla Vecchia, F. M. and Avanzini M. (2002). New findings of isolated remains of Triassic reptiles from Northeastern Italy. Boll. Soc. Paleontol. Ital. *41*, 215–235.
S18. Martin Sander, P., Pérez de Villar, P. R., Furrer, H., & Wintrich, T. (2021). Giant Late Triassic ichthyosaurs from the Kössen Formation of the Swiss Alps and their paleobiological implications. J.Vert. Paleontol. e2046017. 10.1080/02724634.2021.2046017
S19. Motani, R., Manabe, M., and Dong, Z. M. (1999). The status of *Himalayasaurus tibetensis* (Ichthyopterygia). *Paludicola*, *2*, 174–181.
S20. Kear, B. P., Fordyce, R. E., Hiller, N., and Siversson, M. (2018). A palaeobiogeographical synthesis of Australasian Mesozoic marine tetrapods. *Alcheringa 42*, 461–486. 10.1080/03115518.2017.1397428
S21. Balini, M., Jenks, J.F., Martin, R., McRoberts, C.A., Orchard, M.J. and Silberling, N.J. (2015). The Carnian/Norian boundary succession at Berlin-Ichthyosaur State Park (Upper Triassic, central Nevada, USA). Palaontol. Z. *89*, 399–433. 10.1007/s12542-014-0244-2
S22. Montague-Judd, D. (1999) Paleo-upwelling and the distribution of Mesozoic marine reptiles. University of Arizona, PhD dissertation. http://hdl.handle.net/10150/283980
S23. Balini, M., Lucas, S.G., Jenks, J.F. and Spielmann J.A. (2010). Triassic ammonoid biostratigraphy: an overview. Geol. Soc. Spec. Publ. *334*, 221–262. 10.1144/SP334.10
S24. Krystyn, L., Gallet, Y., Besse, J. and Marcoux., J. (2002). Integrated upper Carnian to lower Norian biochronology and implications for the Upper Triassic magnetic polarity time scale. Earth Planet. Sci. Let. *203*, 343–351. 10.1016/S0012-821X(02)00858-0
S25. Channell, J.E.T., Kozur, H.W., Sievers, T., Mock, R., Aubrecht, R., and Sykora, M. (2003). Carnian-Norian biomagnetostratigraphy at Silickà Brezovà (Slovakia): correlation to other Tethyan sections and to the Newark Basin. Palaeogeogr., Palaeoclimatol., Palaeoecol. *191*, 65–109. 10.1016/S0031-0182(02)006545
S26. Muttoni, G., Kent, D.V., Olsen, P.E., Di Stefano, P., Lowrie, W., Bernasconi, S.M., and Hernandez, F.M. (2004). Tethyan magnetostratigraphy from Pizzo Mondello (Sicily) and correlation to the Late Triassic Newark astrochronological polarity time scale. Geol. Soc. Am. Bull. *116*, 1043–1058. 10.1130/B25326.1
S27. Muttoni, G., Meço, S., and Gaetani, M. (2005). Magnetostratigraphy and biostratigraphy of the Late Triassic Guri Zi section, Albania: constraint on the age of the Carnian-Norian boundary. Riv. Ital. Paleontol. Stratigr. *111*, 233–245. 10.13130/2039-4942/6307
S28. Kent, D.V., Olsen, P.E., and Muttoni, G. (2017). Astrochronostratigraphic polarity time scale (APTS) for the Late Triassic and Early Jurassic from continental sediments and correlation with standard marine stages. Earth-Sci. Rev. *166*, 153–180. 10.1016/j.earscirev.2016.12.014
S29. Furin, S., Preto, N., Rigo, M., Roghi, G., Gianolla, P., Crowley, J.L., and Bowring, S.A. (2006). High-precision U-Pb zircon age from the Triassic of Italy: implications for the Triassic time scale and the Carnian origin of calcareous nannoplankton and dinosaurs. Geology *34*, 1009–1012. 10.1130/G22967A.1
S30. Maron, M., Muttoni, G., Dekkers, M.J., Mazza, M., Roghi, G., Breda, A., Krijgsman, W., and Rigo, M. (2017). Contribution to the magnetostratigraphy of the Carnian: new magneto-biostratigraphic constraints from Pignola-2 and Dibona marine sections, Italy. Newsletters on Stratigraphy *50*, 187–203. 10.1127/nos/2017/0291
S31. Grasby, S.E., Them II, T.R., Chen, Z., Yin, R. and Ardakani, O.H. (2019). Mercury as a proxy for volcanic emissions in the geologic record. Earth-Sci. Rev. *196*, 102880. 10.1016/j.earscirev.2019.102880

S32. Percival, L.M.E., Bergquist, B.A., Mather, T.A. and Sanei, H. (2021). Sedimentary mercury enrichments as a tracer of large igneous province volcanism. In Environmental Change and Large Igneous Provinces: The Deadly Kiss of LIPs, R.E. Ernst, A.J. Dickson, A. Bekker, eds. AGU Geophysical Monograph *255*, 247–262. 10.1002/9781119507444.ch11
S33. Greene, A.R., Scoates, J.S., Weis, D., Katvala, E.C., Israel, S. and Nixon, G.T. (2010). The architecture of oceanic plateaus revealed by the volcanic stratigraphy of the accreted Wrangellia oceanic plateau. Geosphere *6*, 47–73. 10.1130/GES00212.1
S34. Tomimatsu, Y., Nozaki, T., Sato, H., Takaya, Y., Kimura, J.I., Chang, Q., Naraoka, H., Rigo, M. and Onoue, T. (2021). Marine osmium isotope record during the Carnian "Pluvial Episode" (Late Triassic) in the pelagic Panthalassa Ocean. Glob. Planet. Change *197*, 103387. 10.1016/j.gloplacha.2020.103387
S35. Dal Corso, J., Bernardi, M., Sun, Y., Song, H., Seyfullah, L.J., Preto, N., Gianolla, P., Ruffell, A., Kustatscher, E., Roghi, G. *et al.* (2020). Extinction and dawn of the modern world in the Carnian (Late Triassic). Sci. Adv. *6*, eaba0099. 10.1126/sciadv.aba0099
S36. Scaife, J.D., Ruhl, M., Dickson, A.J., Mather, T.A., Jenkyns, H.C., Percival, L.M.E., Hesselbo, S.P., Cartwright, J., Eldrett, J.S., Bergman, S.C. *et al.* (2017). Sedimentary mercury enrichments as a marker for submarine large igneous province volcanism? Evidence from the mid-Cenomanian event and Oceanic Anoxic Event 2 (Late Cretaceous). Geochem. Geophys. Geosys. *18*, 4253–4275. 10.1002/2017GC007153
S37. Percival, L.M.E., Jenkyns, H.C., Mather, T.A., Dickson, A.J., Batenburg, S.J., Ruhl, M., Hesselbo, S.P., Barclay, R., Jarvis, I., Robinson, S.A. *et al.* (2018). Does large igneous province volcanism always perturb the mercury cycle? Comparing the records of Oceanic Anoxic Event 2 and the end-Cretaceous to other Mesozoic events. Am. J. Sci., *318*, 799–860. 10.2475/08.2018.01
S38. Percival, L.M.E., Tedeschi, L.R., Creaser, R.A., Bottini, C., Erba, E., Giraud, F., Svensen, H., Savian, J., Trindade, R., Coccioni, R. *et al.* (2021). Determining the style and provenance of magmatic activity during the early Aptian oceanic anoxic event (OAE 1A). Global and Planetary Change *200*, 103461. 10.1016/j.gloplacha.2021.103461
S39. Mazaheri-Johari, M., Gianolla, P., Mather, T.A., Frieling, J., Chu, D. and Dal Corso, J. (2021). Mercury deposition in Western Tethys during the Carnian Pluvial Episode (Late Triassic). Sci. Rep. *11*, 17339. doi.org/10.1038/s41598-021-96890-8
S40. Dickens, G.R., O'Neil, J.R., Rea, D.K. and Owen, R.M. (1995). Dissociation of oceanic methane hydrate as a cause of the carbon isotope excursion at the end of the Paleocene. Paleoceanography *10*, 965–971. 10.1029/95PA02087
S41. Zachos, J. C., Arthur, M. A. and Dean, W. E. (1989). Geochemical evidence for suppression of pelagic marine productivity at the Cretaceous/Tertiary boundary. Nature *337*, 61–64. https://doi.org/10.1038/337061a0